Integrative taxonomy of the Pseudo-nitzschia (Bacillariophyceae) populations in the NW Adriatic Sea, with a focus on a novel cryptic species in the P. delicatissima species complex

Integrative taxonomy of the *Pseudo-nitzschia* (Bacillariophyceae) populations in the NW Adriatic Sea, with a focus on a novel cryptic species in the *P. delicatissima* species complex

SONIA GIULIETTI[1], TIZIANA ROMAGNOLI[1], MELANIA SIRACUSA[2], SIMONE BACCHIOCCHI[2], CECILIA TOTTI[1,3] AND STEFANO ACCORONI[1,2]

[1]*Dipartimento di Scienze della Vita e dell'Ambiente, Università Politecnica delle Marche, via Brecce Bianche, 60131 Ancona*

[2]*Istituto Zooprofilattico Sperimentale Umbria e Marche, Via Cupa di Posatora, 3, 60131 Ancona, Italy*

[3]*Consorzio Interuniversitario per le Scienze del Mare, CoNISMa, ULR Ancona, 60131 Ancona, Italy*

CONTACT

Corresponding author: Stefano Accoroni, s.accoroni@univpm.it

ACKNOWLEDGEMENTS

We are grateful to LTER-ITALY (Italian Long-Term Ecological Research Network) and to ECOSS (Ecological Observing System in the Adriatic Sea) project. Thanks to the crew of M/N Actea for their support during sampling activities. Special thanks to Luigi Gobbi for assistance with the EM.

FUNDING

This research was partially supported by the Italian Ministry of Health (Ricerca Finalizzata 2016) under grant number GR-2016-02363211. The cruises carried out with the M/N Actea were

entirely funded by the Department of Life and Environmental Sciences (Università Politecnica delle Marche).

RUNNING TITLE

Pseudo-nitzschia in the NW Adriatic Sea

ABSTRACT

Species of the genus *Pseudo-nitzschia* are common inhabitants of phytoplankton communities of the northern Adriatic Sea, reaching high abundances. During 2018–2019 a total of 138 cultured *Pseudo-nitzschia* strains were isolated from northwestern Adriatic Sea and were characterized by using both morphological (TEM) and molecular (LSU, ITS, ITS2 secondary structure) approaches. Observation of frustule ultrastructure and phylogenetic analysis resolved a total of six taxa, i.e. *P. fraudulenta*, *P. pungens*, *P. calliantha*, *P. mannii*, *P. delicatissima* and *P.* cf. *arenysensis*. Results of the integrative taxonomic approach clearly revealed that *P.* cf. *arenysensis* is a cryptic species within *P. delicatissima* species complex. *Pseudo-nitzschia* cf. *arenysensis* is closely related to *P. arenysensis*, which forms a subclade and a sister group in LSU and ITS phylogenies, respectively. When comparing ITS2 secondary structure of *P.* cf. *arenysensis* and *P. arenysensis*, 1 CBC, 1 HCBC and 2 SNPs were recognized, suggesting reproductive isolation. Domoic acid production was not detected in any of the studied strains.

KEYWORDS

Cryptic species; Domoic acid; Phylogeny; Secondary structure; Ultrastructure

INTRODUCTION

The focus of scientists on the worldwide-distributed genus *Pseudo-nitzschia* H. Peragallo (Hasle 2002) markedly increased since 1987, when a human illness (named Amnesic Shellfish Poisoning, ASP) related to the consumption of shellfish contaminated by a neurotoxin called Domoic Acid (DA), produced by *Pseudo-nitzschia multiseries* (Hasle) Hasle, was reported for the first time in Prince Edward Island, eastern Canada (Bates *et al.* 1989; Hasle 1995).

In the last decade, a growing number of *Pseudo-nitzschia* species has been described, resulting in 53 currently accepted species (Guiry & Guiry 2020). Within the genus, cryptic species (i.e. those having genetic diversity not associated to morphological differences) or pseudo-cryptic species (i.e. those having minor morphological differences visible only by electron microscopy) are very common. Considering that 27 species are known to produce DA (Lundholm 2020), discriminating different species is a crucial issue.

Traditionally, *Pseudo-nitzschia* species have been subdivided in two groups based on cell width in valve view: all species wider than 3 µm have been combined in the *P. seriata* group, while those less than 3 µm formed the *P. delicatissima* group (Hasle & Syvertsen 1997). The examination by transmission (TEM) and scanning electron microscopy (SEM) of frustule ultrastructure is essential but is not always sufficient for an identification at species level, given the presence of cryptic species. Among the *P. delicatissima* group, 36 cryptic and pseudo-cryptic species have been described to date (Lundholm *et al.* 2003, 2006, 2012; Amato & Montresor 2008; Quijano-Scheggia *et al.* 2009; Lim *et al.* 2012; Teng *et al.* 2015; Percopo *et al.* 2016; Li *et al.* 2017; Ajani *et al.* 2018; Gai *et al.* 2018; Huang *et al.* 2019), and species discernible by electron microscopy have been grouped into two main species complexes, the *P. delicatissima* and *P. pseudodelicatissima* complexes, which differ by having in valve view biseriate and uniseriate striae, respectively (Lundholm *et al.* 2003, 2006).

Molecular taxonomic studies conducted on *Pseudo-nitzschia* species have used several genetic markers (i.e. LSU ribosomal gene, internal transcribed spacer, cytochrome oxidase-1 and the chloroplast-encoded gene for the large subunit of ribulose-1,5-biphosphate carboxylase) (Amato *et al.* 2007; Kaczmarska *et al.* 2008; Casteleyn *et al.* 2009, 2010; Quijano-Scheggia *et al.* 2009; Penna *et al*. 2013; Teng *et al.* 2015; Pugliese *et al*. 2017), but the noncoding internal

transcribed spacer (ITS) region of the nuclear ribosomal operon was shown to be the best tool to separate cryptic and pseudo-cryptic species (Lundholm *et al.* 2003, 2006; Quijano-Scheggia *et al.* 2009; Percopo *et al.* 2016; Huang *et al.* 2019). Indeed, ITS1–ITS2 is a fast evolving genetic marker discriminating between closely related species, and is therefore helpful for low level phylogenetic analysis (Coleman 2003; Schultz *et al.* 2005). In addition, the secondary structure of ITS2 has been widely used as a structural marker in species delimitation (e.g. Coleman 2000, 2009; Wolf *et al.* 2013), as the presence of compensatory base changes (CBCs) or hemi-compensatory base changes (HCBCs) can be used to infer the existence of reproductive isolation in congeneric species (Coleman 2009; Wolf *et al.* 2013) and this has also been used for descriptions of *Pseudo-nitzschia* species (e.g. Amato *et al.* 2007; Lim *et al.* 2012, 2013; Lundholm *et al.* 2012; Teng *et al.* 2014, 2015, 2016; Li *et al.* 2017). Studies on reproductive isolation between closely related species seem to suggest a correlation between mating incompatibility and CBCs: although mating compatibility is not necessarily related to the absence of CBCs (Coleman 2002; Coleman & Vacquier 2002; Amato *et al.* 2007), the presence of at least one CBC seems to be sufficient for having sexual incompatibility (Coleman 2002, 2003; Coleman & Vacquier 2002; Amato *et al.* 2007).

There is an extensive literature concerning phytoplankton distribution and dynamics in the northern Adriatic Sea thanks to the Long-Term Ecological Research (LTER) sites where multiparametric data (e.g. chemical, physical, hydrographic, biological) have been collected for decades (Bernardi Aubry *et al.* 2004, 2012; Cabrini *et al.* 2012; Marić *et al.* 2012; Mozetič *et al.* 2012; Cerino *et al.* 2019; Totti *et al.* 2019), and the seasonality and interannual variability of a number of phytoplankton species has been depicted. However, despite its constant presence within the phytoplankton community of the Adriatic (Caroppo *et al.* 1999; Bernardi Aubry *et al.*

2004, 2006, 2012; Penna *et al.* 2006; Bosak *et al.* 2009; Cabrini *et al.* 2012; Marić *et al.* 2012; Cerino *et al.* 2019; Totti *et al.* 2019; Dermastia *et al.* 2020) and the presence of potentially toxic species, an in-depth characterization of the *Pseudo-nitzschia* population has been performed only in the last decade, in the NW (Penna *et al.* 2013) and in the NE Adriatic Sea (Arapov *et al.* 2020; Dermastia *et al.* 2020).

Among *Pseudo-nitzschia* species recorded in Adriatic Sea several potentially toxic species occur: *P. calliantha* Lundholm, Moestrup & Hasle, *P. delicatissima* (Cleve) Heiden, *P. fraudulenta* (Cleve) Hasle, *P. subfraudulenta* (Hasle) Hasle, *P. galaxiae* Lundholm & Moestrup, *P. pungens* (Grunow *ex* Cleve) Hasle, *P. multistriata* (Takano) Takano and *P. pseudodelicatissima* (Hasle) Hasle (Arapov *et al.* 2016, 2017; Dermastia *et al.* 2020). Nevertheless, in the Adriatic Sea only *P. delicatissima* was found to produce DA and at low levels (0.063 fg cell^{-1} in only one out of 38 cultured strains; Penna *et al.* 2013), and the presence of DA in shellfish has been detected only occasionally since its first record in 2000 (Ciminiello *et al.* 2005; Marić *et al.* 2011; Arapov *et al.* 2016) with concentrations always well below the EU regulatory limit of 20 mg kg^{-1} (Regulation – EC – No 853/2004).

This work represents a first effort to characterize the *Pseudo-nitzschia* population in the coastal station of the Senigallia-Susak transect (NW Adriatic Sea) included in the LTER-Italy, highlighting the species composition, coupling morphological analysis (i.e. LM and TEM), molecular marker analysis (i.e. ITS1–ITS2 and LSU rDNA) and the secondary structure of ITS2. Among the recorded species, *Pseudo-nitzschia* cf. *arenysensis* was revealed as a novel cryptic species within the *P. delicatissima* complex. The toxin content of each species was also analysed.

MATERIAL AND METHODS

Study area and strain isolation

The study area is the coastal station of the Senigallia-Susak transect located in the southern part of the northern Adriatic sub-basin at 1.2 NM from the Italian coastline (bottom depth 12 m) and included in the LTER (Long-Term Ecological Research) Italian sites (SG01 43°45.86′N, 13°13.00′E; Fig. 1).

Sampling was carried out with about a monthly frequency from January 2018 to December 2019 with a phytoplankton net (mesh size 20 µm). The isolation of single cells of *Pseudo-nitzschia* in 24-well plates followed the capillary pipette method (Hoshaw & Rosowski 1973). Cultures were maintained at 21°C with a 12:12 h (light:dark) photoperiod and an irradiance of 100 µmol m^{-2} s^{-1}, in sterile filtered seawater enriched with f/2 nutrients (Guillard & Ryther 1962). Every month, the algal cultures were checked for their purity and quality and refreshed with fresh culture medium. A total of 138 monoclonal *Pseudo-nitzschia* strains were established.

Morphological characterization

LIGHT MICROSCOPY ANALYSIS

Measurements of *Pseudo-nitzschia* cells were carried out using a ZEISS Axiovert 135 inverted microscope (Carl Zeiss AG, Oberkochen, Germany) equipped with phase contrast at ×1000 magnification using a micrometric ocular. Measurements of apical axis (AA) and the overlapping region (in terms of the ratio AA:overlap) were performed on at least 100 cells for each taxon.

TRANSMISSION ELECTRON MICROSCOPY (TEM)

A total of 25 strains were used for ultrastructural analysis (Table S1). Subsamples were collected from cultures (not older than two years from the isolation date) during exponential phase. The collected strains were acid-cleaned following von Stosch's protocol (Hasle & Syvertsen 1997) for TEM analysis. Briefly, samples were centrifuged, the supernatant was removed, then the pellet was resuspended with 1 ml of distilled water in order to remove salt. After that, the cells were cleaned with HNO_3 and H_2SO_4 (1:4 v:v), and washed with distilled water (four times, at least). A drop (2 µl) of the cleaned material was placed on a grid for observation with a Philips CM200 TEM (Philips, Amsterdam, The Netherlands). Several cells were measured (see Table 1) for Transapical Axis (TA), fibulae, striae and poroid density in both valves and cingular bands.

DNA extraction, PCR amplification and sequencing

Of the total 138 strains established, 15 have been used for molecular analyses. Cultures were harvested during late exponential phase and centrifuged at 4000 × g for 15 min and pellets were extracted using CTAB (*N-cetyl-N,N,N*-trimethylammoniumbromide) buffer (2% CTAB, 1 M Tris pH 8.0, 0.5 M EDTA pH 8.0, 5 M NaCl, 1%) modified from Doyle & Doyle (1987).

Extracted DNA was amplified by Polymerase Chain Reaction (PCR), carried out with a SimpliAmp™ Thermal Cycler (Thermo Fisher Scientific, Waltham, MA, USA); PCR amplification of ITS (ITS1–5.8S–ITS2) and LSU (region D1–D3) ribosomal genes was conducted as described in Accoroni *et al.* (2020).

PCR products were visualized under UV in agarose gel (1%), then were purified and directly Sanger-sequenced by Macrogen Europe (Amsterdam, The Netherlands).

Sequence analyses and phylogeny

Sequences were adjusted for the presence of double peaks by eye with BioEdit (Hall 1999). The alignment of LSU and ITS sequences included 15 sequences from this study and 57 and 61 sequences, respectively, from GenBank with the purpose of adding as many *Pseudo-nitzschia* species as possible. Following Huang *et al.* (2019), *Fragilariopsis vanheurckii* (Peragallo) Hustedt (only for LSU alignment), *F. nana* (Steemann Nielsen) Paasche and *F. kerguelensis* (O'Meara) Hustedt were also added to the alignment (Table S2). *Bacillaria paxillifera* (O.F. Müller) Hendey (AF417678) and *Nitzschia navis-varingica* Lundholm & Moestrup (KX353643) were selected as outgroups for LSU and ITS data sets, respectively, based on the findings of Huang *et al.* (2019) and Quijano-Scheggia *et al.* (2020).

Alignments were made with ClustalW (Thompson *et al.* 1994) (https://www.genome.jp/tools-bin/clustalw) with default settings. The resulting LSU and ITS alignments had 911 and 1,140 nucleotides, respectively, and were adjusted manually with Bioedit in order to exclude gaps resulting from non-aligned segments. The final LSU alignment yielded 446 characters, of which 330 conserved and 109 variable sites, and 69 parsimony-informative sites.

The final ITS alignment yielded 829 characters, of which 249 conserved and 566 variable sites, and 486 parsimony-informative sites. The two data sets were analysed by Maximum Likelihood (ML) and Bayesian Inference (BI). The best nucleotide substitution model was tested with Partitionfinder 2 (Lanfear *et al.* 2017). The construction of both ML and BI was conducted with a generalized time-reversible evolution model (GTR) with gamma distribution and invariant sites for BI (GTR+G+I).

ML analysis were carried out with RAxML (Stamatakis *et al.* 2008), with 1,000 pseudoreplicates. Bayesian analyses were carried out using MrBayes 3.2 (Ronquist *et al.* 2012) with 3,000,000 Markov chain Monte Carlo generations, with sample frequency of 1,500 and diagnosing frequency of 1,000. The statistical validity of the Bayesian analysis was checked through Tracer v.1.7 (Rambaut *et al.* 2018). The 50% majority rule consensus tree was constructed discarding the first 25% of the samples. Posterior probabilities were calculated to measure tree strength. Both ML and BI analysis were carried out through Cipress portal (Miller *et al.* 2011). The outputs from the analyses were visualized by FigTree v1.4.4 (Rambaut 2018).

The genetic p-distance value was calculated using MEGA7 (Kumar *et al.* 2016).

ITS2 secondary structure

The ITS2 sequences of the species recovered during this study were annotated with HMMer software (Eddy 1998) using an ITS2 database (http://its2.bioapps.biozentrum.uni-wuerzburg.de/). Secondary structures of ITS2 were predicted using RNAstructure 6.2 (Mathews 2014), with default parameters. The secondary structure showing the typical folding of the genus *Pseudo-nitzschia* (i.e. four helices and one pseudo-helix) and the lowest free energy was selected. The ITS2 secondary structures were aligned using RNAforester (Höchsmann 2005), the presence of compensatory base changes (CBCs) and hemi-compensatory base changes (HCBCs) were checked with 4SALE (Seibel *et al.* 2008) and the structures were visualized with VARNA (Darty *et al.* 2009). When ITS2 sequences did not match any others for homology modelling, their closest relatives indicated by the phylogenetic analysis were used.

Toxin content

CHEMICALS AND STANDARDS

The acetonitrile (MeACN) and formic acid (FA) were of LC-MS grade, and the methanol (MeOH) was of HPLC grade. Water was distilled and passed through a MilliQ water purification system (DIW) (Millipore Ltd., Bedford, MA, USA).

Certified reference material for domoic acid (DA), CRM-DA-g (103.3 µg ml^{-1}), was purchased from the Institute of Biotoxin Metrology at the National Research Council of Canada (NRCC, Halifax, Nova Scotia, Canada). Calibration solutions of DA were prepared from serial dilutions of the reference material in DIW.

DOMOIC ACID EXTRACTION

Chemical analyses of *Pseudo-nitzschia* species requires a large quantity of cells, so each strain was grown in an increasing volume up to a maximum of 2 L to achieve abundances ranging from 4×10^6 to 14×10^9 cells. The strains were grown in the same culture conditions reported above. Cells were harvested from the early stationary growth phase. Pellets of 27 *Pseudo-nitzschia* strains (Table S3) were extracted with 50% methanol in water (*v*:*v*), following the official EU-RL RP-LC-UV method (EURLMB 2008) for the determination of DA in shellfish and finfish.

The entire culture volume (2 L) was centrifuged for 20 min at 2500 × *g* (4°C) in 40 centrifuge tubes (50 ml volume). Pellets were combined and extracted with 5 ml of 50% methanol, vortex-mixed for 1 min, and bath-sonicated for 10 min. After sonication, the aliquot was centrifuged for 10 min at 2500 × *g* (4°C), and the supernatant was transferred to a 100-ml evaporation flask. Pellet extraction was repeated three times, and the supernatants were

combined and evaporated to dryness. The residue was reconstituted in 1 ml of 50% methanol and filtered through a 0.2-µm syringe filter (Minisart, Sartorius, Germany) for LC-MS/MS analysis.

LC-MS/MS ANALYSES

LC-MS/MS analyses were performed using a hybrid triple-quadrupole/linear ion trap 3200 QTRAP mass spectrometer (AB Sciex, Darmstadt, Germany) equipped with a Turbo V source and an electrospray ionization (ESI) probe. The mass spectrometer was coupled to an Agilent model 1200 LC instrument (Palo Alto, CA, USA), which included a solvent reservoir, inline degasser, quaternary pump, refrigerated autosampler and column oven.

The method was implemented following the conditions described by Mafra *et al.* (2009), which were properly modified. LC separation was performed using a Gemini®® NX-C18 column (2 mm × 100 mm, 3 µm particle size; Phenomenex, Torrance, CA, USA), set at 40°C, with a flowrate of 0.4 ml min^{-1}. Mobile phase A was DIW and B was MeACN, both containing 0.2% of FA. Gradient elution was adopted, as described below: from 10% to 20% B in 5 min, from 20% to 35% B in 1 min, then hold for 6 min, return to the original conditions at 13 min, and hold for 7 min before the next injection.

Infusion experiments were performed using CRM-DA-g to set the turbo IonSpray source parameters as follows: Nebulizer Gas (GS1) 50 psi, Auxiliary Gas (GS2) 60 psi, Temperature (TEM) 600°C, Ion Spray Voltage (IS) 5000 V, Curtain Gas (CUR) 20 psi.

Domoic acid was detected using Multiple Reaction Monitoring (MRM) in positive ion mode by selecting the following transitions: *m/z* 312.2→266.1, *m/z* 312.2→220.1, and *m/z* 312.2→161.1. In addition, the pseudotransition *m/z* 334.2→334.2 of sodium adduct $[DA + Na]^+$ was monitored to investigate ion suppression due to salts. A declustering potential (DP) of 60 V

and a collision energy (CE) of 30 V were used for all transitions. LOQ, calculated assuming a signal:noise (S:N) ratio of 10, was 10 ng ml^{-1}, while LOD (S:N ratio of 3) was 3 ng ml^{-1}.

RESULTS

Morphological characterization

During 2018-2019, 138 strains were successfully isolated and identified by LM as belonging to four taxonomic groups: *Pseudo-nitzschia delicatissima* complex, *P. pseudodelicatissima* complex, *P. fraudulenta*, *P. pungens*. Identities were resolved both through electron microscopy (TEM) and molecular analyses, and led to the identification of *P. fraudulenta* and *P. pungens* (of the *P. seriata* group), *P. calliantha* and *P. mannii* Amato & Montresor (of the *P. pseudodelicatissima* complex), and *P. delicatissima* and *P.* cf. *arenysensis* (of the *P. delicatissima* complex).

Pseudo-nitzschia calliantha, *P. delicatissima*, *P. pungens* and *P. mannii* were isolated in winter-spring (the latter also in autumn), while *P. fraudulenta* and *P.* cf. *arenysensis* were isolated only in winter and summer, respectively (Table 1).

SPECIES OF *PSEUDO-NITZSCHIA SERIATA* GROUP

Pseudo-nitzschia fraudulenta (Cleve) Hasle

Cells were lanceolate and symmetrical in valve view, and linear to fusiform in girdle view (Figs 2, 3). Cells formed stepped chains. The AA ranged from 53.8 to 80.7 µm and the TA from 3.5 to 5.3 µm (Table 1). In valve view, the central nodule was visible within a large interspace (as long as 3–5 striae, Fig. 4). Fibulae were 20–24 in 10 µm and striae 22–26 in 10 µm (Table 1). Each stria was bi- or triseriate, with 5–7 poroids in 1 µm (Table 1). Each poroid had 2–7 hymen sectors (Fig. 5). Terminal nodules were located very close to the frustule end (Fig. 6). In girdle view, the valvocopula showed rectangular striae; each stria was 3 poroids wide and up to 8 poroids high (Fig. 7). The number of band striae in the valvocopula was 36–42 in 10 µm (Table 1).

Pseudo-nitzschia pungens (Grunow *ex* Cleve) Hasle

Cells were linear in valve view and fusiform in girdle view (Figs 8, 9), strongly silicified, with interstriae and fibulae discernible by LM. The AA ranged from 51.1 to 99.4 µm and the TA from 2.0 to 3.6 µm (Table 1). Cells were symmetrical in valve view (Figs 8, 9) or slightly asymmetrical. The central nodule was absent. The number of fibulae and striae in 10 µm was 5–18 and 9–16, respectively (Table 1). Each stria was generally biseriate with rounded poroids (1–4 poroids in 1 µm) without hymen sectors (Figs 10, 11) (Table 1). Frequently, additional poroids between the two rows of poroids were observed (Figs 10, 11). In girdle view, three cingular bands were visible. The valvocopula was perforated by square, oval and rectangular poroids (Figs 12, 13), frequently divided by 1–2 hymen sectors (Fig. 12). Dimensions and shape of poroids did not differ much between valvocopula and the second band, but the second band had more striae than the valvocopula (Fig. 13). Poroid dimensions became smaller in the abvalvar direction (Fig. 13). Band striae ranged from 12 to 23 in 10 µm (Table 1).

SPECIES OF THE *PSEUDO-NITZSCHIA PSEUDODELICATISSIMA* COMPLEX

Pseudo-nitzschia calliantha Lundholm, Moestrup & Hasle

Cells were linear in both valve and girdle view (Figs 14, 15), with tips narrowing towards ends. Cells formed stepped chains (Fig. 14). The AA was 61–120 µm and the TA 1.5–2.1 µm (Table 1). In valve view, the raphe was interrupted by the central nodule with a central interspace (Fig. 16). The valve had 14–24 fibulae and 34–38 striae in 10 µm (Table 1). Striae were uniseriate with 4–6 rounded poroids in 1 µm (Table 1) perforated in 2–7 hymen sectors, frequently arranged in a flower-like pattern, which is a distinctive feature of this species (Figs 16, 17). Proximal and distal mantles were uniseriate, also with flower-like pattern (Fig. 17). In girdle view, the cingulum showed three bands with striae ranging from 44 to 46 in 10 µm (Table 1). The valvocopula was 3–4 poroids high and 2–3 poroids wide (Fig. 18). The second band was 2–3 poroids high and 2–3 poroids wide (Fig. 19). The third band was scarcely silicified and was 2 poroids high and 1–2 poroids wide. Frequently, some small poroids were present below the second and the third band stria (Fig. 19).

Pseudo-nitzschia mannii Amato & Montresor

Cells were linear in both valve and girdle view, with tips narrowing towards ends (Figs 20, 21). Cells formed stepped chains. The AA ranged from 34 to 120 µm and the TA from 1.6 to 2.6 µm (Table 1). In valve view, the central nodule was visible (Fig. 22). The number of fibulae was 18–25 in 10 µm and the number of striae was 32–36 in 10 µm (Table 1). Striae were uniseriate with 4–5 poroids in 1 µm (Table 1) with hymen perforated by 2–6 sectors with a radial arrangement (Fig. 23). Three cingular bands were

visible in girdle view, with the number of band striae ranging from 38 to 45 in 10 µm (Table 1). The valvocopula had biseriate striae 2–3 poroids high; an additional poroid between the two rows was frequently present (Figs 24, 25). The second band had biseriate striae 1–2 poroids high (Fig. 24).

SPECIES OF THE *PSEUDO-NITZSCHIA DELICATISSIMA* COMPLEX

***Pseudo-nitzschia delicatissima* (Cleve) Heiden**

Cells were characterized by a linear shape in valve view and a slightly sigmoid shape with truncated ends in girdle view (Figs 26, 27). Cells formed stepped chains (Fig. 26). The AA ranged from 29 to 71 µm and the TA from 0.8 to 1.8 µm (Table 1). In valve view, the central nodule was visible with a large central interspace (Fig. 28). The raphe ended as a thin linear slit in both the central and terminal nodules (Figs 28, 29). The number of fibulae was 22–30 in 10 µm and the number of striae was 38–49 in 10 µm (Table 1). Each stria was biseriate with 5–11 poroids in 1 µm (Table 1). Poroids had an irregular shape without hymen sectors (Fig. 30). In girdle view, the cingulum consisted of three girdle bands with a number of band striae ranging from 45 to 54 in 10 µm (Table 1). The valvocopula had striae with one poroid, characterized by 1–2 hymen sectors (Fig. 31). The second band was two poroids high; in abvalvar direction, the upper poroid was characterized by 1–2 hymen sectors with irregular shapes, while the lower poroid was smaller and had no hymen sectors (Fig. 31). The third band was smooth (Fig. 31).

Pseudo-nitzschia* cf. *arenysensis

Cells had a linear shape in valve view and a slightly sigmoid shape with truncated ends in girdle view (Figs 32, 33). Frustules were scarcely silicified. In culture, cells formed short (2–4 cells) stepped chains. The AA ranged from 29.1 to 50.6 µm and the TA from 1.5 to 2.3 µm (Table 1). In valve view, the central nodule was visible with a large interspace. Fibulae and striae were regularly spaced, with density of striae higher than that of fibulae (Fig. 34). The number of fibulae in 10 µm was 16–36 and the number of striae was 36–42 (Table 1). Each stria was biseriate with 8–12 poroids in 1 µm (Table 1). Poroids had irregular shapes without hymen sectors and were located close to the interstriae (Fig. 35). Both central and terminal parts of the raphe ended with a thin linear slit (Figs 34, 36). In girdle view, the cingulum was composed by three girdle bands with 42–52 band striae in 10 µm (Table 1). The valvocopula had striae with one poroid characterized by 2–4 hymen sectors (Figs 37, 38). The second band was 2 poroids high. Poroids were small and had irregular shapes (Figs 37, 38). In abvalvar direction, the lower poroid was similar (Fig. 37) or less marked and smaller (Fig. 38) than the upper one. The third band was either smooth (Fig. 38) or had small and barely visible poroids (Fig. 37).

Molecular analyses

Phylogenetic trees inferred from ML and BI analyses of LSU and ITS rDNA showed the same topology. ML and BI analyses revealed that strains from this study were grouped in six moderately supported (>93 and 0.94 bootstrap values and posterior probabilities, respectively) clades (i.e. *P. calliantha*, *P. fraudulenta*, *P. mannii*, *P. pungens*, *P. delicatissima* and *P.* cf. *arenysensis*) based on LSU, except for *P. delicatissima* (only supported by BI analysis) and *P. fraudulenta* (only supported by ML analysis) (Fig. 39).

ML and BI analysis inferred from ITS revealed that strains from this study were grouped in six strongly supported (>95 and 0.97 bootstrap values and posterior probabilities, respectively) clades (i.e. *P. calliantha*, *P. delicatissima*, *P. fraudulenta*, *P. mannii*, *P. pungens* clade I and *P.* cf. *arenysensis*) (Fig. 40).

Phylogenies based on LSU and ITS showed *P.* cf. *arenysensis* strains clustering together in a well-supported clade (LSU: 93/0.99, ITS: 100/1 bootstrap values and posterior probabilities, respectively). While in the LSU tree *P.* cf. *arenysensis* was resolved in a strongly supported clade with *P. arenysensis* Quijano-Scheggia, Garcés & Lundholm as subclade (91/0.9), in the ITS tree *P.* cf. *arenysensis* strains clustered separately as a sister group to *P. arenysensis* (99/1).

The LSU rDNA phylogeny showed *P.* cf. *arenysensis* strains from this study clustering with three other strains of *Pseudo-nitzschia* (LT596179, LT596180 and LT596192) from Adriatic Sea and with two other strains (KC801041 and KC801042) from the Tyrrhenian Sea; the *p*-distance between *P.* cf. *arenysensis* from this study and the above five strains was 0.001, whereas the distance from *P. arenysensis* was 0.002.

Similarly, the ITS rDNA phylogeny showed *P.* cf. *arenysensis* strains from this study clustering with three other strains of *Pseudo-nitzschia* (LT596194, LT596195 and LT596202)

from Adriatic Sea; the *p*-distance between *P.* cf. *arenysensis* from this study and these three strains was 0.000, whereas the distance from *P. arenysensis* was 0.092.

ITS2 secondary structure analyses

The classical four helices, with an additional helix IIa, was recovered in the ITS2 secondary structure of all species examined. In detail, the total length of ITS2 of *P.* cf. *arenysensis* from this study was 267 bases with a 46.5% of GC content. The secondary structure of *P.* cf. *arenysensis* from this study (Fig. 41) was compared with the sequence of *P. arenysensis* (strain AY764136) recovered from GenBank. Helix I was 33 bases in length with 1 HCBC (U:A ↔U:G on nucleotide 28), 2 SNPs (G ↔ A and U ↔ A, on nucleotides 24 and 25, respectively; the latter changed the folding of the tip of helix I), 1 CBC (G:U ↔ C:G) and deletion of 5 base pairs. Helix II was 27 bases in length with a SNP (C ↔ U, on nucleotide 50). Helix IIa was 23 bases in length and no differences were detected between *P.* cf. *arenysensis* and *P. arenysensis*. Helix III was 122 bases in length with 4 SNPs (C ↔ A, U ↔ C, U ↔ A, U ↔ C, on nucleotides 120, 179, 180 and 181, respectively) and a deletion of a single nucleotide (G) changing the folding of a portion of helix III. Helix IV was 25 bases in length with 1 HCBC (U:G ↔ U:A on nucleotide 240), a SNP (A ↔ U on nucleotide 244) and the deletion of 8 base pairs and a single nucleotide. A SNP was detected on nucleotide 228 (A ↔ C).

Toxin content

Analyses of toxin content involved 27 cultured strains isolated from different periods: 13 *P. delicatissima*, 3 *P.* cf. *arenysensis*, 3 *P. calliantha*, 4 *P. pungens*, 2 *P. mannii* and 2 *P. fraudulenta*.

None of the strains tested by LC-MS/MS produced DA in detectable amounts; the LOD varied between 0.75 and 0.00021 fg cell^{-1}.

DISCUSSION

In recent years, several studies addressed the ecology and the specific composition of the genus *Pseudo-nitzschia* in the Mediterranean Sea, due to its importance in the phytoplankton communities (Caroppo *et al.* 2005; Quijano-Scheggia *et al.* 2008; Sahraoui *et al.* 2009; Penna *et al*. 2013; Ruggiero *et al.* 2015; Arapov *et al.* 2020; Dermastia *et al.* 2020) and to its potential involvement in ASP (Ljubešić *et al.* 2011; Busch *et al.* 2016; Melliti Ben Garali *et al.* 2020). Unfortunately, because of the crypticity and, therefore, the difficulty to identify species of this genus by both LM and EM, knowledge about the ecological behaviour is limited either to *Pseudo-nitzschia* as a whole or to the classical groups or complexes easily identifiable by LM. However, species may differ, for example, regarding seasonality, relationship with environmental parameters and toxicity, and so discriminating different species is of crucial importance.

This study represents a first effort to characterize the *Pseudo-nitzschia* population in the coastal station of the LTER Senigallia-Susak transect in northwestern Adriatic Sea, using an integrated approach combining morphological and molecular data. Monthly isolations of the highest possible number of strains were performed in order to obtain a reliable estimation of the *Pseudo-nitzschia* species composition in the area. This approach led to isolate 138 strains which clustered in six distinct genetic lineages, i.e. *P. delicatissima*, *P. calliantha*, *P. mannii*, *P. pungens* clade I (as proposed by Casteleyn et al. (2008)), *P. fraudulenta* and *P.* cf. *arenysensis* (a cryptic species within the *P. delicatissima* complex). Unfortunately, although *P. multistriata* and

P. cf. *galaxiae* have been often identified under LM in the long-term data set (Totti *et al.* 2019), those species were not found during the study period.

In general, the morphological data of *Pseudo-nitzschia* species obtained in this study matched those reported in the literature (Caroppo *et al.* 2005; Ljubešić *et al.* 2011; Moschandreou *et al.* 2012; Grbin *et al.* 2017; Dermastia *et al.* 2020), with only few exceptions. *Pseudo-nitzschia mannii* revealed a lower density of band striae in 10 µm (38–45) than in the original description (46–47; Amato & Montresor 2008) and *P. fraudulenta* had a smaller TA (3.5–5.3 µm) and higher density of poroids (5–7 in 1 µm) than in the original description (5–6 and 4–5, respectively; Hasle *et al.* 1996). Moreover, *P. pungens* from our study area showed a number of morphometric details differing from those retrieved from literature as highlighted by Accoroni *et al.* (2020). *P. pungens* contains three genetically distinct groups (clade I, II and III), based on sequences of rDNA internal transcribed spacers (ITS) region, and three varieties (*P. pungens* var. *pungens*, var. *cingulata* and var. *aveirensis*) distinguishable based on morphological characters (Casteleyn *et al*. 2008; Churro *et al*. 2009). However, a clade does not necessarily correspond to a morphological variety and *vice versa*: clade II comprises both *P. pungens* var. *pungens* and var. *cingulata*, while clade III comprises both *P. pungens* var. *pungens* and var. *aveirensis* (Lim *et al.* 2014); moreover, *P. pungens* clade I from this study showed a wide morphological variability that matched with at least two varieties, i.e. *P. pungens* var. *pungens* and var. *aveirensis* (Accoroni *et al*. 2020).

To date the *P. delicatissima* complex comprises 11 species: *Pseudo-nitzschia bucculenta* Gai, Hedemand, Lundholm & Moestrup, *P. decipiens* Lundholm & Moestrup, *P. dolorosa* Lundhlom & Moestrup, *P. galaxiae, P. hainanensis* Xiu Mei Chen & Yang Li, *P. hallegraeffii* P. Ajani, A. Verma & Sh. Murray, *P. micropora* Priisholm, Moestrup & Lundholm, *P. multistriata*,

P. sabit S.T. Teng, H.C. Lim, P.T. Lim & Leaw, and the two cryptic species *P. arenysensis* and *P. delicatissima*.

Regarding *P.* cf. *arenysensis* observed in this study, this seems to be a new cryptic species within the *delicatissima* complex (Percopo *et al.* in prep.). Morphological data of all species of *P. delicatissima* complex are reported in Table 2 for comparison purposes; only *P. multistriata* and *P. sabit* were not included since their valve shapes are well distinguishable by LM (i.e. sigmoid and falcate, respectively; Takano 1995; Teng *et al.* 2015). The Adriatic *P.* cf. *arenysensis* was distinguishable from *P. bucculenta*, *P. dolorosa* and *P. hallegraeffii* by the symmetry of the valve and from *P. micropora* by the presence of the central nodule (not recorded in *P. micropora*). The main morphometrical data of *P.* cf. *arenysensis* from the Adriatic matched those of the other species of the complex, except for: (i) the TA (1.5–2.3 µm) that was lower than that reported in *P. bucculenta*, *P. dolorosa* and *P. hallegraeffii* (2.7–3.6, 2.5–3.0 and 2.2–3.0 µm, respectively); (ii) the wider range of density of fibulae (16–36 in 10 µm) than all the others; (iii) the higher density of striae (36–42 in 10 µm) than *P. bucculenta* and *P. dolorosa* (28–35 and 30–36 in 10 µm, respectively), but lower than *P. decipiens*, *P. galaxiae* and *P. micropora* (41–46, 56–64 and 41–46 in 10 µm, respectively); (iv) higher density of poroids (8–12 in 1 µm) than *P. bucculenta*, *P. dolorosa* and *P. hallegraeffii* (5–7.5, 5–8 and 6–8 in 1 µm); (v) higher density of band striae (42–52 in 10 µm) than *P. bucculenta* (38–39 in 10 µm). The LSU and ITS sequences clustered with those of Lamari *et al.* (2013) (KC801041 and KC801042, reported as *P.* cf. *delicatissima*) and Pugliese *et al.* (2017) (LSU: LT596179, LT596180 and LT596192; ITS: LT596194, LT596195 and LT596202, reported as *P.* cf. *arenysensis*). Although in the LSU tree *P. arenysensis* and *P.* cf. *arenysensis* were not resolved into two separated clades, the ITS tree resolved these two species into two well-supported clades, confirming that

the ITS region of the nuclear ribosomal operon is the best tool to separate cryptic species within the *Pseudo-nitzschia delicatissima* complex (Lundholm *et al.* 2003, 2006; Quijano-Scheggia *et al.* 2009; Percopo *et al.* 2016; Huang *et al.* 2019).

The separation of *P.* cf. *arenysensis* from *P. arenysensis* was further supported considering the comparison of the secondary structure of the ITS2. Secondary structure information in the ITS2 transcript has been used widely as a structural marker in species delimitation, as the presence of CBCs can be used to infer the existence of reproductive isolation in congeneric species (Coleman 2009; Wolf *et al.* 2013). This has also been used for descriptions of *Pseudo-nitzschia* species (e.g. Coleman 2002, 2003; Coleman & Vacquier 2002; Amato *et al.* 2007; Lim *et al.* 2012, 2013; Lundholm *et al.* 2012; Teng *et al.* 2014, 2015, 2016; Li *et al.* 2017). The analysis of the secondary structure of the ITS2 of *P.* cf. *arenysensis* strains from this study shows several changes in nucleotides (i.e. CBCs, HCBCs and SNPs) and deletions compared to its closest relative *P. arenysensis*, supporting the reproductive isolation of *P.* cf. *arenysensis* (Coleman 2002, 2003; Coleman & Vacquier 2002; Amato *et al.* 2007).

Pseudo-nitzschia cf. *arenysensis* in this study was isolated once in late summer. However, its presence had been already reported in the Gulf of Naples in summer (as *P.* cf. *delicatissima*, Lamari *et al*. 2013) and in winter-autumn in NW Adriatic Sea (as *P*. cf. *arenysensis*, Pugliese *et al.* 2017).

The importance of discriminating different species becomes even more necessary when within the same group are gathered potentially toxic species and non-harmful species. In the Adriatic Sea, DA was recorded for the first time by Ciminiello *et al.* (2005) in *Mytilus galloprovincialis* with a toxin content that ranged from 63 to 190 ng g^{-1}, well below the regulatory limit of DA in tissue (20 mg kg^{-1}) (Regulation (EC) No 854/2004). Since then, DA

was revealed in a few occasions, rarely reaching 2 mg kg^{-1} in tissue (Ljubešić *et al.* 2011; Marić *et al.* 2011; Arapov *et al.* 2017), therefore finding a DA producer in NW Adriatic Sea was not expected.

Among the six species isolated during the present study, *P. pungens*, *P. fraudulenta*, *P. delicatissima* and *P. calliantha* have been reported to be toxic elsewhere (Hasle 2002; Lundholm *et al.* 2003; Moschandreou *et al.* 2012). However, in this study none of the tested strains produced DA in detectable amounts. Indeed, several of these potentially toxic species have been reported to be non-toxic (Trainer *et al.* 2012), and in particular in the NW Adriatic strains where DA has been detected only in *P. delicatissima* and in very low concentration (0.063 fg $cell^{-1}$, Penna *et al.* 2013).

In contrast, in the NE Adriatic Sea, although DA concentration in both net and seawater samples were under the detection limit, the occurrence of a *P. calliantha* bloom has been linked to DA accumulation in shellfish, with a maximum DA concentration of 1.32 µg DA g^{-1} of tissue (Marić *et al.* 2011). Very low levels of DA were recently detected in *P. multistriata* (0.2 fg $cell^{-1}$) in the Gulf of Trieste (Dermastia *et al.* 2018).

This study confirmed no DA production by *P. mannii* (Amato & Montresor 2008) and highlighted the non-toxicity of *P.* cf. *arenysensis*. However, the observed differences in toxin production by the same species in different studies may perhaps be also the result of different culture conditions and other environmental factors, or they may depend on the sensitivity of the analysis method. Indeed, field and laboratory studies have shown that there are several factors (e.g. excess light, different nitrogen sources with a combination of silicate or phosphorus limitation) that influence the production of DA (Husson *et al.* 2016; Thorel *et al.* 2017; Pednekar *et al.* 2018; Bates *et al.* 2019).

REFERENCES

Accoroni S., Giulietti S., Romagnoli T., Siracusa M., Bacchiocchi S. & Totti C. 2020. Morphological variability of *Pseudo-nitzschia pungens* clade I (Bacillariophyceae) in the northwestern Adriatic Sea. *Plants* 9: 1420. DOI:10.3390/plants9111420.

Ajani P.A., Verma A., Lassudrie M., Doblin M.A. & Murray S.A. 2018. A new diatom species *P. hallegraeffii* sp. nov. belonging to the toxic genus *Pseudo-nitzschia* (Bacillariophyceae) from the East Australian Current. *PLOS One* 13: Article e0195622. DOI: https://doi.org/10.1371/journal.pone.0195622.

Amato A. & Montresor M. 2008. Morphology, phylogeny, and sexual cycle of *Pseudo-nitzschia mannii* sp. nov. (Bacillariophyceae): a pseudo-cryptic species within the *P. pseudodelicatissima* complex. *Phycologia* 47: 487–497.

Amato A., Kooistra W.H.C.F., Ghiron J.H.L., Mann D.G., Pröschold T. & Montresor M. 2007. Reproductive isolation among sympatric cryptic species in marine diatoms. *Protist* 158: 193–207. DOI: 10.1016/j.protis.2006.10.001.

Arapov J., Ujević I., Pfannkuchen D.M., Godrijan J., Bakrač A., Gladan Ž.N. & Marasović I. 2016. Domoic acid in phytoplankton net samples and shellfish from the Krka River estuary in the Central Adriatic Sea. *Mediterranean Marine Science* 17: 340–350.

Arapov J., Skejić S., Bužančić M., Bakrač A., Vidjak O., Bojanić N., Ujević I. & Gladan Ž.N. 2017. Taxonomical diversity of *Pseudo- nitzschia* from the Central Adriatic Sea. *Phycological Research* 65: 280–290.

Arapov J., Bužančić M., Skejić S., Mandić J., Bakrač A., Straka M. & Ninčević Gladan Ž. 2020. Phytoplankton dynamics in the Middle Adriatic Estuary, with a focus on the potentially toxic genus *Pseudo-nitzschia*. *Journal of Marine Science and Engineering* 8: Article 608. DOI: doi:10.3390/jmse8080608.

Bates S.S., Bird C.J, Freitas A.S.W., de Foxall R., Gilgan M., Hanic L.A., Johnson G.R., McCulloch A.W., Odense P. & Pocklington R. 1989. Pennate diatom *Nitzschia pungens* as

the primary source of domoic acid, a toxin in shellfish from eastern Prince Edward Island, Canada. *Canadian Journal of Fisheries and Aquatic Sciences* 46: 1203–1215.

Bates S.S., Lundholm N., Hubbard K.A., Montresor M. & Leaw C.P. 2019. Toxic and harmful marine diatoms. In: *Diatoms: fundamentals and applications* (Ed. by J. Seckbach & R. Gordon), pp 389–434. Scrivener Publishing LLC.

Bernardi Aubry F., Berton A., Bastianini M., Socal G. & Acri F. 2004. Phytoplankton succession in a coastal area of the NW Adriatic, over a 10-year sampling period (1990–1999). *Continental Shelf Research* 24: 97–115. DOI:10.1016/j.csr.2003.09.007.

Bernardi Aubry F., Acri F., Bastianini M., Bianchi F., Cassin D., Pugnetti A. & Socal G. 2006. Seasonal and interannual variations of phytoplankton in the Gulf of Venice (Northern Adriatic Sea). *Chemistry and Ecology* 22: 71–91. DOI:10.1080/02757540600687962.

Bernardi Aubry F., Cossarini G., Acri F., Bastianini M., Bianchi F., Camatti E., De Lazzari A., Pugnetti A., Solidoro C. & Socal G. 2012. Plankton communities in the northern Adriatic Sea: patterns and changes over the last 30 years. *Estuarine, Coastal and Shelf Science* 115: 125–137. DOI:10.1016/j.ecss.2012.03.011.

Bosak S., Burić Z., Djakovac T. & Viličić D. 2009. Seasonal distribution of plankton diatoms in Lim Bay, northeastern Adriatic sea. *Acta Botanica Croatica* 68: 351–365.

Busch J.A., Andree K.B., Diogène J., Fernández-Tejedor M., Toebe K., John U., Krock B., Tillmann U. & Cembella A.D. 2016. Toxigenic algae and associated phycotoxins in two coastal embayments in the Ebro Delta (NW Mediterranean). *Harmful Algae* 55: 191–201.

Cabrini M., Fornasaro D., Cossarini G., Lipizer M. & Virgilio D. 2012. Phytoplankton temporal changes in a coastal northern Adriatic site during the last 25 years. *Estuarine, Coastal and Shelf Science* 115: 113–124. DOI:10.1016/j.ecss.2012.07.007

Caroppo C., Fiocca A., Sammarco P. & Magazzù G. 1999. Seasonal variations of nutrients and phytoplankton in the coastal SW Adriatic Sea (1995-1997). *Botanica Marina* 42: 389–400. DOI:10.1515/BOT.1999.045.

Caroppo C., Congestri R., Bracchini L. & Albertano P. 2005. On the presence of *Pseudo-nitzschia calliantha* Lundholm, Moestrup et Hasle and *Pseudo-nitzschia delicatissima* (Cleve) Heiden in the Southern Adriatic Sea (Mediterranean Sea, Italy). *Journal of Plankton Research* 27: 763–774.

Casteleyn G., Chepurnov VA., Leliaert F., Mann D.G., Bates S.S., Lundholm N., Rhodes L., Sabbe K. & Vyverman W. 2008. *Pseudo-nitzschia pungens* (Bacillariophyceae): a cosmopolitan diatom species? *Harmful Algae* 7: 241–257. DOI: 10.1016/j.hal.2007.08.004.

Casteleyn G., Adams N.G., Vanormelingen P., Debeer A.E., Sabbe K. & Vyverman W. 2009. Natural hybrids in the marine diatom *Pseudo-nitzschia pungens* (Bacillariophyceae): genetic and morphological evidence. *Protist* 160: 343–354. DOI:10.1016/j.protis.2008.11.002.

Casteleyn G., Leliaert F., Backeljau T., Debeer A.E., Kotaki Y., Rhodes L., Lundholm N., Sabbe K. & Vyverman W. 2010. Limits to gene flow in a cosmopolitan marine planktonic diatom. *Proceedings of the National Academy of Sciences of the United States of America* 107: 12952–12957. DOI:10.1073/pnas.1001380107.

Cerino F., Fornasaro D., Kralj M., Giani M. & Cabrini M. 2019. Phytoplankton temporal dynamics in the coastal waters of the north-eastern Adriatic Sea (Mediterranean Sea) from 2010 to 2017. *Nature Conservation* 34: 343–372. DOI: 10.3897/natureconservation.34.30720.

Churro C.I., Carreira C.C., Rodrigues F.J., Craveiro S.C., Calado A.J., Casteleyn G. & Lundholm N. 2009. Diversity and abundance of potentially toxic *Pseudo-nitzschia* Peragallo in Aveiro coastal lagoon, Portugal and description of a new variety, *P. pungens* var. *aveirensis* var. nov. *Diatom Research* 24: 35–62.

Ciminiello P., Dell'Aversano C., Fattorusso E., Forino M., Magno G.S., Tartaglione L., Quilliam M.A., Tubaro A. & Poletti R. 2005. Hydrophilic interaction liquid chromatography/mass spectrometry for determination of domoic acid in Adriatic shellfish. *Rapid Communications in Mass Spectrometry* 19: 2030–2038. DOI:10.1002/rcm.2021.

Coleman A.W. 2000. The significance of a coincidence between evolutionary landmarks found in mating affinity and a DNA sequence. *Protist* 151: 1–9. DOI: 10.1078/1434-4610-00002.

Coleman A.W. 2002. Comparison of *Eudorina*/*Pleodorina* ITS sequences of isolates from nature with those from experimental hybrids. *American Journal of Botany* 89: 1523–1530.

Coleman A.W. 2003. ITS2 is a double-edged tool for eukaryote evolutionary comparisons. *Trends in Genetics* 19: 370–375.

Coleman A.W. 2009. Is there a molecular key to the level of "biological species" in eukaryotes? A DNA guide. *Molecular Phylogenetics and Evolution* 50: 197–203.

Coleman A.W. & Vacquier V.D. 2002. Exploring the phylogenetic utility of ITS sequences for animals: a test case for abalone (*Haliotis*). *Journal of Molecular Evolution* 54: 246–257.

Darty K., Denise A. & Ponty Y. 2009. VARNA: Interactive drawing and editing of the RNA secondary structure. *Bioinformatics* 25: 1974–1975. DOI: 10.1093/bioinformatics/btp250.

Dermastia T.T., Stanković D., Francé J., Žnidarič Tušek M., Ramšak A. & Mozetič P. 2018. Diversity of *Pseudo-nitzschia* H. Peragallo, 1900 along the Slovenian coast, Adriatic Sea, with insights into seasonality, toxicity and potential introductions. In: *Harmful Algae 2018 – from ecosystems to socioecosystems. Proceedings of the 18th International Conference on Harmful Algae* (Ed. by P. Hess), pp 72–75. International Society for the Study of Harmful Algae, 2020.

Dermastia T.T., Cerino F., Stanković D., Francé J., Ramšak A., Tušek M.Ž., Beran A., Natali V., Cabrini M. & Mozetič P. 2020. Ecological time series and integrative taxonomy unveil seasonality and diversity of the toxic diatom *Pseudo-nitzschia* H. Peragallo in the northern Adriatic Sea. *Harmful Algae* 93: Article 101773.

Doyle J.J. & Doyle J.L. 1987. A rapid DNA isolation procedure for small quantities of fresh leaf tissue. *Phytochemical Bulletin* 19: 11–15. DOI:citeulike-article-id:678648.

Eddy S.R. 1998. Profile hidden Markov models. *Bioinformatics* 14: 755–763.

EURLMB 2008. EU-Harmonised Standard Operating Procedure for determination of domoic acid in shellfish and finfish by RP-HPLC using UV detection. Version 1, June 2008. https://www.aesan.gob.es/CRLMB/docs/docs/procedimientos/EU-Harmonised-SOP-ASP-HPLC-UV_Version1.pdf; searched on 23 December 2020.

European Council 2004. Regulation (EC) No 853/2004 of the European Parliament and of the Council of 29 April 2004 laying down specific hygiene rules for on the hygiene of foodstuffs. *Official Journal of the European Union* L139/1, 47: 55–205.

Gai F.F., Hedemand C.K., Louw D.C., Grobler K., Krock B., Moestrup Ø. & Lundholm N. 2018. Morphological, molecular and toxigenic characteristics of Namibian *Pseudo-nitzschia* species – including *Pseudo-nitzschia bucculenta* sp. nov. *Harmful Algae* 76: 80–95.

Grbin D., Pfannkuchen M., Babić I., Mejdandžić M., Mihanović H., Marić Pfannkuchen D., Godrijan J., Peharec Štefanić P., Olujić G. & Ljubešić Z. 2017. Multigene phylogeny and morphology of newly isolated strain of *Pseudo-nitzschia mannii* Amato & Montresor (Adriatic Sea). *Diatom Research* 32: 127–131.

Guillard R.R.L. & Ryther J.H. 1962. Studies of marine planktonic diatoms: I. *Cyclotella nana* Hustedt, and *Detonula confervacea* (Cleve) Gran. *Canadian Journal of Microbiology* 8: 229–239. DOI:10.1139/m62-029.

Guiry M.D. & Guiry G.M. 2020. AlgaeBase. World-wide electronic publication. National University of Ireland, Galway. In *AlgaeBase. World-Wide Electronic Publication, National University of Ireland, Galway.*

Hall T.A. 1999. BioEdit: a user-friendly biological sequence alignment editor and analysis program for Windows 95/98/NT. *Nucleic Acids Symposium Series* 41: 95–98.

Hasle G.R. 1995. *Pseudo-nitzschia pungens* and *P. multiseries* (Bacillariophyceae): Nomenclatural history, morphology and distribution. *Journal of Phycology* 31: 428–435. DOI:10.1111/j.0022-3646.1995.00428.x.

Hasle G.R. 2002. Are most of the domoic acid-producing species of the diatom genus *Pseudo-nitzschia* cosmopolites? *Harmful Algae* 1: 137–146. DOI:10.1016/S1568-9883(02)00014-8.

Hasle G.R. & Syvertsen E.E. 1997. Chapter 2 – Marine Diatoms. In: *Identifying Marine Phytoplankton* (Ed. by C. Tomas), pp 5–385, Academic Press, San Diego (USA).

Hasle G.R., Lange C.B. & Syvertsen E.E. 1996. A review of *Pseudo-nitzschia*, with special reference to the Skagerrak, North Atlantic, and adjacent waters. *Helgoländer Meeresuntersuchungen* 50: 131–175. DOI:10.1007/BF02367149.

Höchsmann M. 2005. The tree alignment model: algorithms, implementations and applications for the analysis of RNA secondary structures. Thesis. Bielefeld University, Bielefeld (Germany). 207 pp.

Hoshaw W. & Rosowski J.R. 1973. Methods for microscopic algae. In: *Handbook of Phycological Methods: Culture Methods and Growth Measurements* (Ed. by J.R. Stein), pp 53–68. Cambridge: Cambridge University Press.

Huang C.X., Dong H.C., Lundholm N., Teng S.T., Zheng G.C., Tan Z.J., Lim P.T. & Li Y. 2019. Species composition and toxicity of the genus *Pseudo-nitzschia* in Taiwan Strait, including *P. chiniana* sp. nov. and *P. qiana* sp. nov. *Harmful Algae* 84: 195–209.

Husson B., Hernández-Fariñas T., Le Gendre R., Schapira M. & Chapelle A. 2016. Two decades of *Pseudo-nitzschia* spp. blooms and king scallop (*Pecten maximus*) contamination by domoic acid along the French Atlantic and English Channel coasts: seasonal dynamics, spatial heterogeneity and interannual variability. *Harmful Algae* 51: 26–39. DOI:https://doi.org/10.1016/j.hal.2015.10.017.

Kaczmarska I., Reid C., Martin J.L. & Moniz M.B.J. 2008. Morphological, biological, and molecular characteristics of the diatom *Pseudo-nitzschia delicatissima* from the Canadian Maritimes. *Botany* 86: 763–772. DOI:10.1139/B08-046.

Kumar S., Stecher G. & Tamura K. 2016. MEGA7: Molecular Evolutionary Genetics Analysis Version 7.0 for Bigger Datasets. *Molecular Biology and Evolution* 33: 1870–1874. DOI:10.1093/molbev/msw054.

Lamari N., Ruggiero M.V., D'Ippolito G., Kooistra W.H.C.F., Fontana A. & Montresor M. 2013. Specificity of lipoxygenase pathways supports species delineation in the marine diatom genus *Pseudo-nitzschia*. *PLOS One* 8: Article e73281. DOI:10.1371/journal.pone.0073281.

Lanfear R., Frandsen P.B., Wright A.M., Senfeld T. & Calcott B. 2017. Partitionfinder 2: New methods for selecting partitioned models of evolution for molecular and morphological phylogenetic analyses. *Molecular Biology and Evolution* 34: 772–773. DOI:10.1093/molbev/msw260.

Li Y., Huang C.X., Xu G.S., Lundholm N., Teng S.T., Wu H. & Tan Z. 2017. *Pseudo-nitzschia simulans* sp. nov. (Bacillariophyceae), the first domoic acid producer from Chinese waters. *Harmful Algae* 67: 119–130. DOI:10.1016/j.hal.2017.06.008.

Lim H., Leaw C., Su S.N., Teng S., Usup G., Mohammad- Noor N., Lundholm N., Kotaki Y. & Lim P. 2012. Morphology and molecular characterization of *Pseudo- nitzschia* (Bacillariophyceae) from Malaysian Borneo, including the new species *Pseudo- nitzschia circumpora* sp. nov. *Journal of Phycology* 48: 1232–1247.

Lim H.C., Teng S.T., Leaw C.P. & Lim P.T. 2013. Three novel species in the *Pseudo- nitzschia pseudodelicatissima* complex: *P. batesiana* sp. nov., *P. lundholmiae* sp. nov., and *P. fukuyoi* sp. nov. (Bacillariophyceae) from the Strait of Malacca, Malaysia. *Journal of Phycology* 49: 902–916.

Lim H.C., Lim P.T., Teng S.T., Bates S.S. & Leaw C.P. 2014. Genetic structure of *Pseudo-nitzschia pungens* (Bacillariophyceae) populations: implications of a global diversification of the diatom. *Harmful Algae* 37:142–52.

Ljubešić Z., Bosak S., Viličić D., Borojević K.K., Marić D., Godrijan J., Ujević I., Peharec P. & Dakovac T. 2011. Ecology and taxonomy of potentially toxic *Pseudo-nitzschia* species in Lim Bay (north-eastern Adriatic Sea). *Harmful Algae* 10: 713–722. DOI:10.1016/j.hal.2011.06.002.

Lundholm N. 2020. Bacillariophyceae, in *IOC-UNESCO Taxonomic Reference List of Harmful Micro Algae*. Available online at http://www.marinespecies.org/hab.

Lundholm N. & Moestrup Ø. 2002. The marine diatom *Pseudo-nitzschia galaxiae* sp. nov. (Bacillariophyceae): morphology and phylogenetic relationships. *Phycologia* 41: 594–605. DOI:10.2216/i0031-8884-41-6-594.1.

Lundholm N., Moestrup Ø., Hasle GR. & Hoef- Emden K. 2003. A study of the *Pseudo-nitzschia pseudodelicatissima*/*cuspidata* complex (Bacillariophyceae): what is *P. pseudodelicatissima*? *Journal of Phycology* 39: 797–813.

Lundholm N., Moestrup Ø., Kotaki Y., Hoef- Emden K., Scholin C. & Miller P. 2006. Inter and intraspecific variation of *Pseudo-nitzschia delicatissima* complex (Bacillariophyceae) illustrated by rRNA probes, morphological data and phylogenetic analyses. *Journal of Phycology* 42: 464–481.

Lundholm N., Bates S.S., Baugh K.A., Bill B.D., Connell L.B., Léger C. & Trainer V.L. 2012. Cryptic and pseudo-cryptic diversity in diatoms-with descriptions of *Pseudo-nitzschia hasleana* sp. nov. and *P. fryxelliana* sp. nov. *Journal of Phycology* 48: 436–454. DOI:10.1111/j.1529-8817.2012.01132.x.

Mafra L.L., Léger C., Bates S.S. & Quilliam M.A. 2009. Analysis of trace levels of domoic acid in seawater and plankton by liquid chromatography without derivatization, using UV or mass spectrometry detection. *Journal of Chromatography A* 1216: 6003–6011. DOI:10.1016/j.chroma.2009.06.050.

Marić D., Ljubešić Z., Godrijan J., Viličić D., Ujević I. & Precali R. 2011. Blooms of the potentially toxic diatom *Pseudo-nitzschia calliantha* Lundholm, Moestrup & Hasle in coastal waters of the northern Adriatic Sea (Croatia). *Estuarine, Coastal and Shelf Science* 92: 323–331. DOI:10.1016/j.ecss.2011.01.002.

Marić D., Kraus R., Godrijan J., Supić N., Djakovac T. & Precali R. 2012. Phytoplankton response to climatic and anthropogenic influences in the north-eastern Adriatic during the last four decades. *Estuarine, Coastal and Shelf Science* 115: 98–112.

Mathews D.H. 2014. RNA secondary structure analysis using RNAstructure. *Current Protocols in Bioinformatics* 46: 12–16.

Melliti Ben Garali S., Sahraoui I., de la Iglesia P., Chalghaf M., Diogène J., Ksouri J. & Sakka Hlaili A. 2020. Factors driving the seasonal dynamics of *Pseudo-nitzschia* species and domoic acid at mussel farming in the SW Mediterranean Sea. *Chemistry and Ecology* 36: 66–82.

Miller M.A., Pfeiffer W. & Schwartz T. 2011. The CIPRES science gateway: a community resource for phylogenetic analyses. In: *Proceedings of the 2011 TeraGrid Conference: Extreme Digital Discovery* 41: 1–8. DOI: https://doi.org/10.1145/2016741.2016785.

Moschandreou K.K., Baxevanis A.D., Katikou P., Papaefthimiou D., Nikolaidis G. & Abatzopoulos T.J. 2012. Inter- and intra-specific diversity of *Pseudo-nitzschia* (Bacillariophyceae) in the northeastern Mediterranean. *European Journal of Phycology* 47: 321–339. DOI:10.1080/09670262.2012.713998.

Mozetič P., Francé J., Kogovšek TŠ., Talaber I. & Malej A. 2012. Plankton trends and community changes in a coastal sea (northern Adriatic): bottom-up vs. top-down control in relation to environmental drivers. *Estuarine, Coastal and Shelf Science* 115: 138–148. DOI:10.1016/j.ecss.2012.02.009.

Pednekar S.M., Bates S.S., Kerkar V. & Matondkar S.G.P. 2018. Environmental factors affecting the distribution of *Pseudo-nitzschia* in two monsoonal estuaries of Western India and effects of salinity on growth and domoic acid production by *P. pungens*. *Estuaries and Coasts* 41: 1448–1462. DOI:https://doi.org/10.1007/s12237-018-0366-y.

Penna A., Ingarao C., Ercolessi M., Rocchi M. & Penna N. 2006. Potentially harmful microalgal distribution in an area of the NW Adriatic coastline: sampling procedure and correlations with environmental factors. *Estuarine, Coastal and Shelf Science* 70: 307–316. DOI:10.1016/j.ecss.2006.06.023.

Penna A., Casabianca S., Perini F., Bastianini M., Riccardi E., Pigozzi S. & Scardi M. 2013. Toxic *Pseudo-nitzschia* spp. in the northwestern Adriatic Sea: characterization of species composition by genetic and molecular quantitative analyses. *Journal of Plankton Research* 35: 352–366.

Percopo I., Ruggiero M.V., Balzano S., Gourvil P., Lundholm N., Siano R., Tammilehto A., Vaulot D. & Sarno D. 2016. *Pseudo-nitzschia arctica* sp. nov., a new cold-water cryptic complex. *Journal of Phycology* 52: 184–199.

Priisholm K., Moestrup Ø. & Lundholm N. 2002. Taxonomic notes on the marine diatom genus *Pseudo-nitzschia* in the Andaman Sea near the island of Phuket, Thailand, with a description of *Pseudo-nitzschia micropora* sp. nov. *Diatom Research* 17: 153–175.

Pugliese L., Casabianca S., Perini F., Andreoni F. & Penna A. 2017. A high resolution melting method for the molecular identification of the potentially toxic diatom *Pseudo-nitzschia* spp. in the Mediterranean Sea. *Scientific Reports* 7: 4259. DOI:10.1038/s41598-017-04245-z.

Quijano-Scheggia S., Garcés E., Flo E., Fernandez-Tejedor M., Diogène J. & Camp J. 2008. Bloom dynamics of the genus *Pseudo-nitzschia* (Bacillariophyceae) in two coastal bays (NW Mediterranean Sea). *Scientia Marina* 72: 577–590.

Quijano-Scheggia S.I., Garcés E., Lundholm N., Moestrup Ø., Andree K. & Camp J. 2009. Morphology, physiology, molecular phylogeny and sexual compatibility of the cryptic *Pseudo-nitzschia delicatissima* complex (Bacillariophyta), including the description of *P. arenysensis* sp. nov. *Phycologia* 48: 492–509. DOI:10.2216/08-21.1.

Quijano-Scheggia S.I., Olivos-Ortiz A., Garcia-Mendoza E., Sánchez-Bravo Y., Sosa-Avalos R., Salas Marias N. & Lim H.C. 2020. Phylogenetic relationships of *Pseudo-nitzschia subpacifica* (Bacillariophyceae) from the Mexican Pacific, and its production of domoic acid in culture. *PLOS One* 15: Article e0231902.

Rambaut A. 2018. FigTree, v. 1.4.4 a graphical viewer of phylogenetic trees. http://tree.bio.ed.ac.uk/software/figtree/.

Rambaut A., Drummond A.J., Xie D., Baele G. & Suchard M.A. 2018. Posterior summarization in Bayesian phylogenetics using Tracer 1.7. *Systematic Biology* 67: 901–904.

Ronquist F., Teslenko M., van der Mark P., Ayres D.L., Darling A., Höhna S., Larget B., Liu L., Suchard M.A. & Huelsenbeck J.P. 2012. MrBayes 3.2: efficient Bayesian phylogenetic

inference and model choice across a large model space. *Systematic Biology* 61: 539–542. DOI:10.1093/sysbio/sys029.

Ruggiero M.V., Sarno D., Barra L., Kooistra W.H.C.F., Montresor M. & Zingone A. 2015. Diversity and temporal pattern of *Pseudo-nitzschia* species (Bacillariophyceae) through the molecular lens. *Harmful Algae* 42: 15–24. DOI:10.1016/j.hal.2014.12.001.

Sahraoui I., Hlaili A.S., Mabrouk H.H., Leger C. & Bates S.S. 2009. Blooms of the diatom genus *Pseudo-nitzschia* H. Peragallo in Bizerte lagoon (Tunisia, SW Mediterranean). *Diatom Research* 24: 175–190.

Schultz J., Maisel S., Gerlach D., Müller T. & Wolf M. 2005. A common core of secondary structure of the internal transcribed spacer 2 (ITS2) throughout the Eukaryota. *RNA* 11: 361–364.

Seibel P.N., Müller T., Dandekar T. & Wolf M. 2008. Synchronous visual analysis and editing of RNA sequence and secondary structure alignments using 4SALE. *BMC Research Notes* 1: Article 91.

Stamatakis A., Hoover P. & Rougemont J. 2008. A rapid bootstrap algorithm for the RAxML web servers. *Systematic Biology* 57: 758–771.

Takano H. 1995. *Pseudo-nitzschia multistriata* (Takano) Takano, a new combination for the pennate diatom *Nitzschia multistriata* Takano. *Diatom (Tokyo)* 10: 73–74.

Teng S.T., Lim H.C., Lim P.T., Dao V.H., Bates S.S. & Leaw C.P. 2014. *Pseudo-nitzschia kodamae* sp. nov. (Bacillariophyceae), a toxigenic species from the strait of Malacca, Malaysia. *Harmful Algae* 34: 17–28. DOI:10.1016/j.hal.2014.02.005.

Teng S.T., Lim P.T., Lim H.C., Rivera- Vilarelle M., Quijano- Scheggia S., Takata Y., Quilliam M.A., Wolf M., Bates S.S. & Leaw C.P. 2015. A non- toxigenic but morphologically and phylogenetically distinct new species of *Pseudo- nitzschia*, *P. sabit* sp. nov. (Bacillariophyceae). *Journal of Phycology* 51: 706–725.

Teng S.T., Tan S.N., Lim H.C., Dao V.H., Bates S.S. & Leaw C.P. 2016. High diversity of *Pseudo-nitzschia* along the northern coast of Sarawak (Malaysian Borneo), with descriptions of *P. bipertita* sp. nov. and *P. limii* sp. nov. (Bacillariophyceae). *Journal of Phycology* 52: 973–989. DOI:10.1111/jpy.12448

Thompson J.D., Higgins D.G. & Gibson T.J. 1994. CLUSTAL W: Improving the sensitivity of progressive multiple sequence alignment through sequence weighting, position-specific gap penalties and weight matrix choice. *Nucleic Acids Research* 22: 4673–4680. DOI:10.1093/nar/22.22.4673

Thorel M., Claquin P., Schapira M., Le Gendre R., Riou P., Goux D., Le Roy B., Raimbault V., Deton-Cabanillas A.-F. & Bazin P. 2017. Nutrient ratios influence variability in *Pseudo-nitzschia* species diversity and particulate domoic acid production in the Bay of Seine (France). *Harmful Algae* 68: 192–205.

Totti C., Romagnoli T., Accoroni S., Coluccelli A., Pellegrini M., Campanelli A., Grilli F. & Marini M. 2019. Phytoplankton communities in the northwestern Adriatic Sea: interdecadal variability over a 30-years period (1988–2016) and relationships with meteoclimatic drivers. *Journal of Marine Systems* 193: 137–153. DOI:10.1016/j.jmarsys.2019.01.007.

Trainer V.L., Bates S.S., Lundholm N., Thessen A.E., Cochlan W.P., Adams N.G. & Trick C.G. 2012. *Pseudo-nitzschia* physiological ecology, phylogeny, toxicity, monitoring and impacts on ecosystem health. *Harmful Algae* 14: 271–300. DOI:10.1016/j.hal.2011.10.025.

Wolf M., Chen S., Song J., Ankenbrand M. & Müller T. 2013. Compensatory base changes in ITS2 secondary structures correlate with the biological species concept despite intragenomic variability in ITS2 sequences – a proof of concept. *PLOS One* 8: Article e66726.

TABLES AND FIGURES

Table 1. Morphometric and ultrastructure data of the six *Pseudo-nitzschia* species retrieved in this study. Seasons of the isolation are shown. (W: winter; SP: spring; SU: summer; A: autumn). Average values (mean ± standard deviation) are reported in parentheses.

Species	Isolation seasons	Apical axis (µm)	Transapical axis (µm)	AA/overlap	Striae in 10 µm	Fibulae in 10 µm	Poroids in 1 µm	Band striae in 10 µm
Pseudo-nitzschia calliantha	W, SP	61–120 (90.1 ± 20.4) n=101	1.5–2.1 (1.8 ± 0.17) n=12	3–13.9 (7.2 ± 2.1) n=101	34–38 (36.4 ± 1.2) n=12	14–24 (19.7 ± 2.6) n=10	4–6 (4.8 ± 0.7) n=14	44–46 (44.8 ± 0.9) n=4
Pseudo-nitzschia delicatissima	W, SP	29–71 (47.7 ± 9.8) n=110	0.8–1.8 (1.4 ± 0.3) n=26	4.3–18.3 (9.6 ± 2.9) n=110	38–49 (41 ± 2.3) n=25	22–30 (26 ± 2.3) n=25	5–11 (8 ± 2.1) n=11	45–54 (50 ± 2.2) n=10
Pseudo-nitzschia fraudulenta	W	53.8–80.7 (71.5 ± 4.8) n=101	3.5–5.3 (4.4 ± 0.4) n=19	3.3–11.6 (6.1 ± 1.8) n=101	22–26 (24 ± 1) n=19	20–24 (22 ± 1.3) n=18	5–7 (6 ± 0.6) n=17	36–42 (38 ± 1.4) n=13
Pseudo-nitzschia mannii	W, SP, A	34–120 (93.4 ± 14.7) n=126	1.6–2.6 (2.0 ± 0.3) n=15	3.2–14.8 (7.2 ± 1.8) n=126	32–36 (34 ± 1.7) n=13	18–25 (20 ± 2.5) n=13	4–5 (4.5 ± 0.5) n=15	38–45 (42 ± 2.4) n=18
Pseudo-nitzschia pungens	W, SP	51–99.4 (78.9 ± 11.7) n=213	2.0–3.6 (2.8 ± 0.3) n=80	2.9–5.9 (3.9 ± 0.6) n=130	5–18 (11.6± 1.9) n=79	9–16 (11.3± 1.2) n=81	1–4 (3 ± 0.6) n=90	12–23 (16.2 ± 2.7) n=88
Pseudo-nitzschia cf. *arenysensis*	SU	29.1–50.6 (38.5 ± 5.2) n=178	1.5–2.3 (1.86 ± 0.17) n=110	5–13 (8.8 ± 1.5) n=104	36–42 (38.3 ± 1.6) n=114	16–36 (21.5 ± 2.2) n=114	8–12 (10.1 ± 0.9) n=61	42–52 (46.0 ± 2.3) n=49

Table 2. Morphometric and ultrastructure data of *Pseudo-nitzschia* species of the *P. delicatissima* complex and resembling to *P.* cf. *arenysensis*. Average values (mean ± standard deviation) are reported in parentheses.

Species	Overlap	Shape	Apical axis (µm)	Transapical axis (µm)	Fibulae in 10 µm	Striae in 10 µm	Rows of poroids in each stria	Poroids in 1 µm	Central nodule	Band Striae	References
Pseudo-nitzschia arenysensis	n.r.	Linear–lanceolate	38.8–58.8 (51.7±6.3)	1.6–2.5 (2±0.3)	20–26 (22.4±1.8)	34–43 (38.7±2.5)	2	7–12	+	40–50 (41.8±1.6)	Quijano-Scheggia *et al.* 2009
Pseudo-nitzschia bucculenta	n.r.	Lanceolate asymmetrical	19–31 (24.9±3.6)	2.7–3.6 (3.0±0.3)	16–21 (18.4±1.2)	28–35 (31.4±1.7)	1–2	5–7.5 (6.7±0.6)	+	38–39 (38±0.6)	Gai *et al.* 2018
Pseudo-nitzschia decipiens	n.r.	Lanceolate	29–64	1.4–2.4 (1.9±0.3)	20–26 (24.0±1.4)	41–46 (43.2±1.2)	2	9–13 (11.4±1.2)	+	48–55 (51.8±1.7)	Lundholm *et al.* 2006
Pseudo-nitzschia delicatissima	n.r.	Lanceolate	19–76	1.4–2.1 (1.8±0.2)	18–26 (21.4±1.6)	34–41 (36.8±1.5)	2	8–12 (10.1±1.2)	+	43–48 (44.2±1.6)	Lundholm *et al.* 2006
Pseudo-nitzschia dolorosa	n.r.	Lanceolate asymmetrical	30–59	2.5–3.0 (2.6±0.2)	18–22 (20.0±1.0)	30–36 (34.5±1.4)	1–2	5–8 (6.6±0.8)	+	40–44 (42.0±1.4)	Lundholm *et al.* 2006
Pseudo-nitzschia galaxiae	n.r.	Lanceolate	25–41	1.2–1.7	16–26	56–64	Several	Several	+	n.r.	Lundholm & Moestrup 2002
Pseudo-nitzschia hallegraeffii	~1/9	Lanceolate asymmetrical	25.6–44.3 (39±3.8)	2.2–3.0 (2.6±0.2)	19–22 (20.0±1.0)	34–39 (36.2±1.4)	2(1)	6–8 (7.6±0.6)	+	46–50 (48±1.6)	Ajani *et al.* 2018
Pseudo-nitzschia micropora	n.r.	Lanceolate	31–57	1.3–2.0	21–29	41–46	2	9–12	–	48–54	Priisholm *et al.* 2002

n.r.: not reported.

LEGENDS FOR FIGURES

Fig. 1. The LTER Senigallia transect in the northern Adriatic Sea. The study station is highlighted by the circle.

Figs 2–7. *Pseudo-nitzschia fraudulenta*, LM (Figs 2, 3) and TEM (Figs 4–7); images obtained from strain 031824.

Fig. 2. Colony of cells in girdle view. Scale bar = 20 µm.

Fig. 3. Colony of cells in valve view. Scale bar = 20 µm.

Fig. 4. Middle part of the valve; arrow indicates the central nodule within a large interspace. Scale bar = 2 µm.

Fig. 5. Valve view showing triseriate striae: circle indicates a poroid divided into 7 sectors. Scale bar = 1 µm.

Fig. 6. Valve view of cell tip with terminal nodule. Scale bar = 1 µm.

Fig. 7. Valvocopula with rectangular triseriate striae. Scale bar = 1 µm.

Figs 8–13. *Pseudo-nitzschia pungens*, LM (Figs 8, 9) and TEM (Figs 10–13).

Fig. 8. Colony in girdle view. Strain 04197. Scale bar = 20 µm.

Fig. 9. Colony in valve view. Strain 01185. Scale bar = 20 µm.

Fig. 10. Middle part of valve with biseriate striae and proximal mantle on the left of raphe slit; circle indicates an additional poroid. Strain 01186. Scale bar = 1 µm.

Fig. 11. Valve view, details of stria showing two additional poroids in the area of the stria close to the raphe. Strain 01186. Scale bar = 1 µm.

Fig. 12. Valvocopula with oval to rectangular poroids; circle indicates a poroid divided in two sectors. Strain 01185. Scale bar = 1 µm.

Fig. 13. Part of cingulum: (vc) valvocopula with rectangular to square poroids and (II) second band with oval to rectangular, smaller poroids. Strain 01186. Scale bar = 1 µm.

Figs 14–19. *Pseudo-nitzschia calliantha*, LM (Figs 14, 15) and TEM (Figs 16–19).

Fig. 14. Colony in girdle view. Strain 12182. Scale bar = 20 µm.

Fig. 15. Colony in valve view. Strain 12182. Scale bar = 20 µm.

Fig. 16. Details of central part of valve showing the central nodule (arrow) within a large interspace. Strain 12184. Scale bar = 1 µm.

Fig. 17. Detail of central part of valve with the proximal (p) and distal (d) mantle. Strain 12184. Scale bar = 1 µm.

Fig. 18. Cingulum with valvocopula (vc). Strain 12181. Scale bar = 1 µm.

Fig. 19. Cingulum with second (II) and third (III) girdle bands. Below the second and the third band stria, some small poroids are present (arrowheads). Strain 12181. Scale bar = 1 µm.

Figs 20–25. *Pseudo-nitzschia mannii*, LM (Figs 20, 21) and TEM (Figs 22–25).

Fig. 20. Colony in girdle view. Strain 06182. Scale bar = 20 µm.

Fig. 21. Colony in valve view. Strain 06182. Scale bar = 20 µm.

Fig. 22. Middle part of valve with central nodule (black arrow) within a large interspace. Strain 031826. Scale bar = 2 µm.

Fig. 23. Detail of poroids of the valve with hymen sectors arranged in circular pattern. Strain 06184. Scale bar = 0.2 µm.

Fig. 24. Valvocopula (vc) and second girdle band (II). Strain 031826. Scale bar = 1 µm.

Fig. 25. Cingulum with valvocopula (vc), second (II) and third (III) girdle bands. Strain 06184. Scale bar = 1 µm.

Figs 26–31. *Pseudo-nitzschia delicatissima*, LM (Figs 26, 27) and TEM (Figs 28–31).

Fig. 26. Colony of four cells in girdle view. Strain 04189. Scale bar = 20 µm.

Fig. 27. Colony of two cells in valve view. Strain 04189. Scale bar = 20 µm.

Fig. 28. Part of valve showing the large central nodule (black arrow) within an interspace. Strain 031815. Scale bar = 2 µm.

Fig. 29. Cell tip with terminal nodule. Strain 031815. Scale bar = 1 µm.

Fig. 30. Middle part of valve with details of biseriate striae. Strain 031816. Scale bar = 0.2 µm.

Fig. 31. Cingular bands: (vc) valvocopula; (II) second cingular band; (III) third cingular band. White circle indicates a poroid without hymen sectors among other hymenate poroids. Strain 031816. Scale bar = 1 µm.

Figs 32–38. *Pseudo-nitzschia* cf. *arenysensis*, LM (Figs 32, 33) and TEM (Figs 34–38).

Fig. 32. Colony of four cells in girdle view. Strain 091911. Scale bar = 20 µm.

Fig. 33. Colony of two cells in valve view. Strain 091911. Scale bar = 20 µm.

Fig. 34. Middle part of valve with the central large interspace; arrow indicates central nodule. Strain 091910. Scale bar = 1 µm.

Fig. 35. Middle part of valve showing biseriate striae with poroids very close to the interstriae. Strain 091910. Scale bar = 0.5 µm.

Fig. 36. Cell tip with terminal nodule. Strain 091910. Scale bar = 1 µm.

Figs 37, 38. Cingular bands: (vc) valvocopula, (II) second cingular band and (III) third cingular band. Images obtained from strains 091916 and 091910, respectively. Scale bar = 0.5 µm.

Fig. 39. Bayesian consensus tree based on LSU D1–D3 sequences. Bayesian inference posterior probabilities (PP) ≥ 0.90 and bootstraps values (ML) ≥ 70% are shown (PP/ML). Strains in bold indicate sequences obtained in this study.

Fig. 40. Bayesian consensus tree based on ITS1–ITS2 sequences. Bayesian inference posterior probabilities (PP) ≥ 0.90 and bootstraps values (ML) ≥ 70% are shown (PP/ML). Strains in bold indicate sequences obtained in this study.

Fig. 41. ITS2 secondary structure of strain 09192 (GenBank code MW580582) of *Pseudo-nitzschia* cf. *arenysensis*. White roman numbers with black background designate the helices. The boxes indicate the structural variations found in *P.* cf. *arenysensis* compared to *P. arenysensis*. Deletions of nucleotides are marked with red background, while changes in nucleotides (i.e. CBCs, HCBCs and SNPs) are marked with blue background.

Fig. 1

Click here to access/download;Figure;Fig 1.tiff

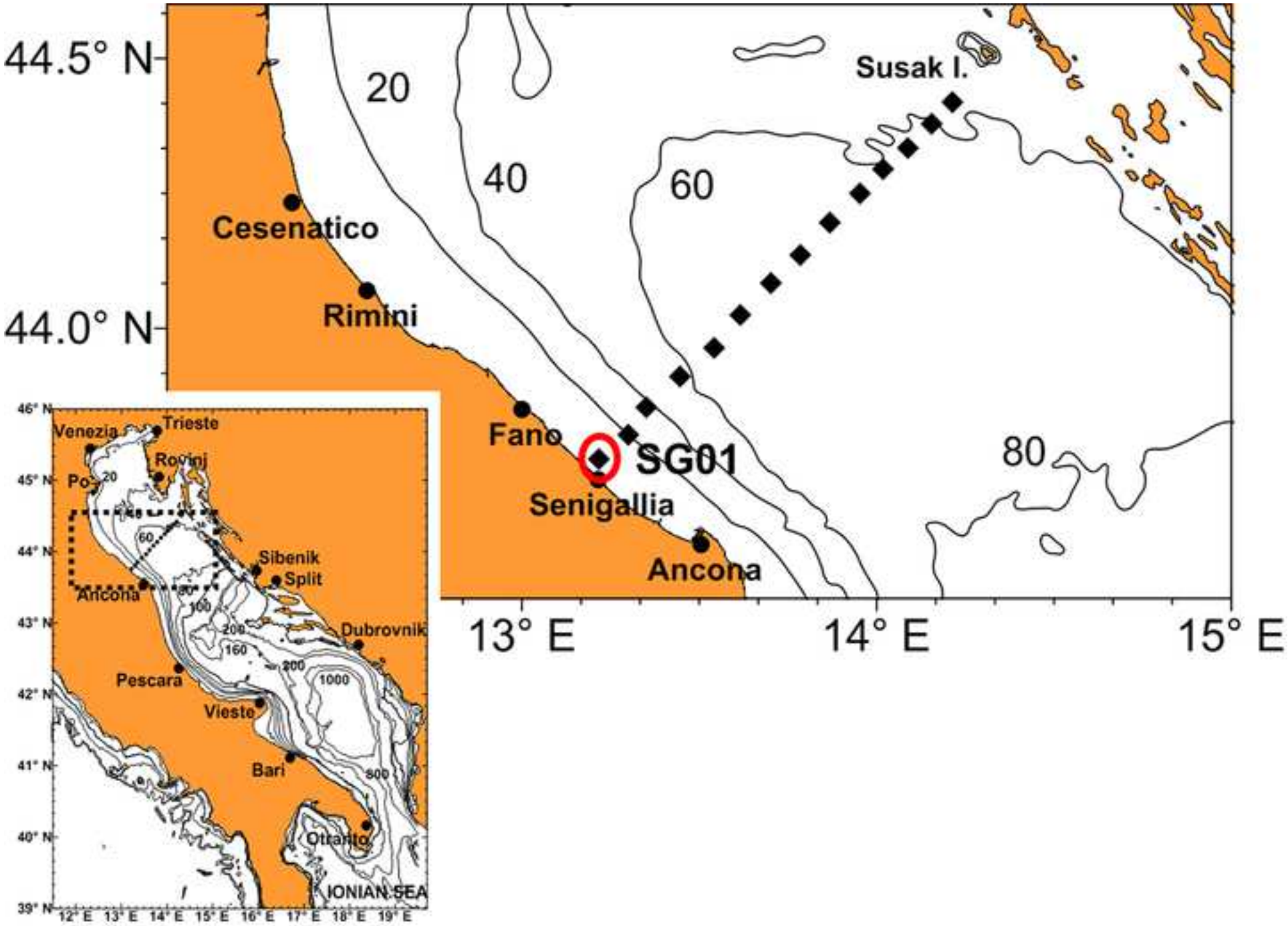

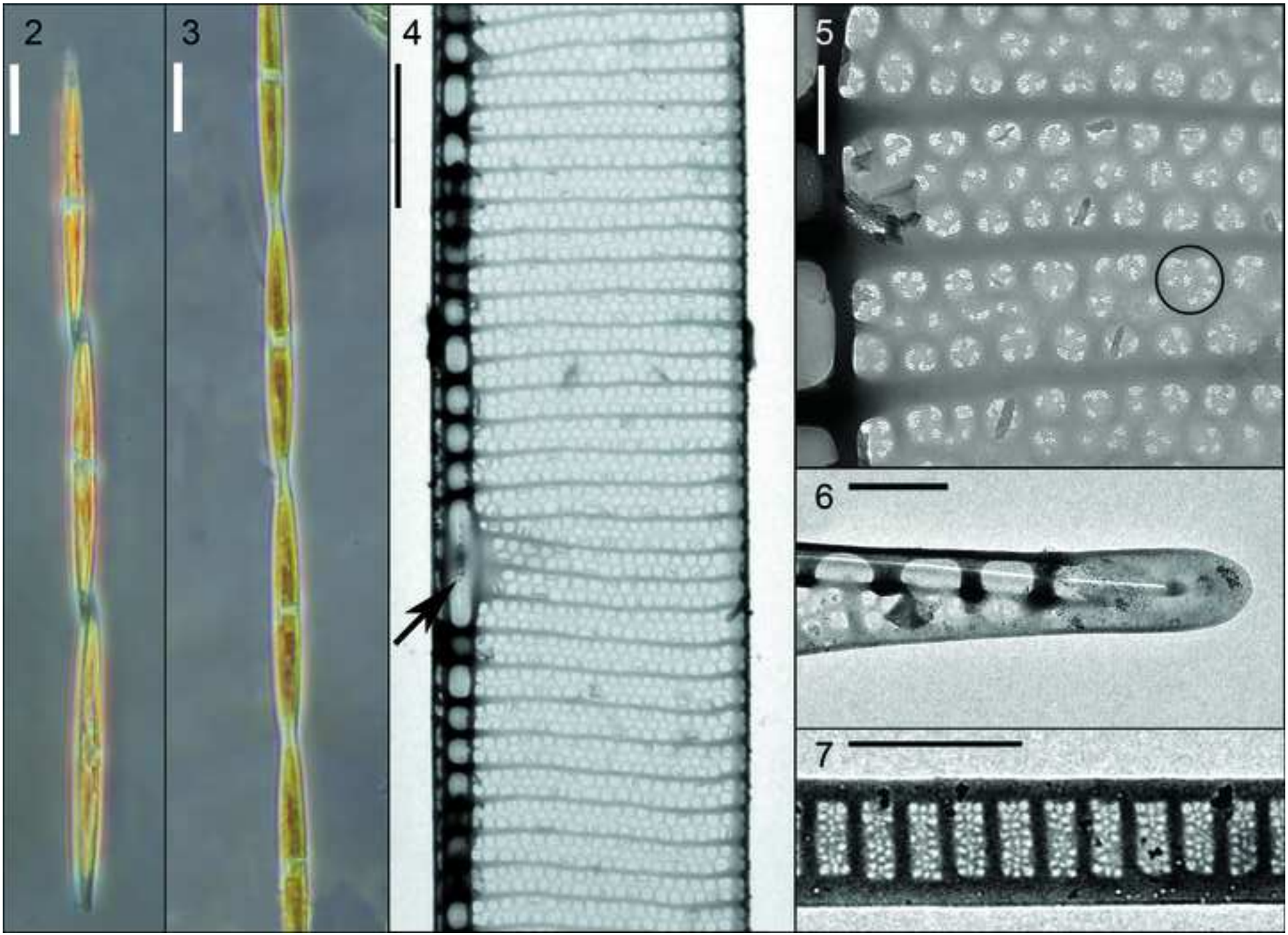

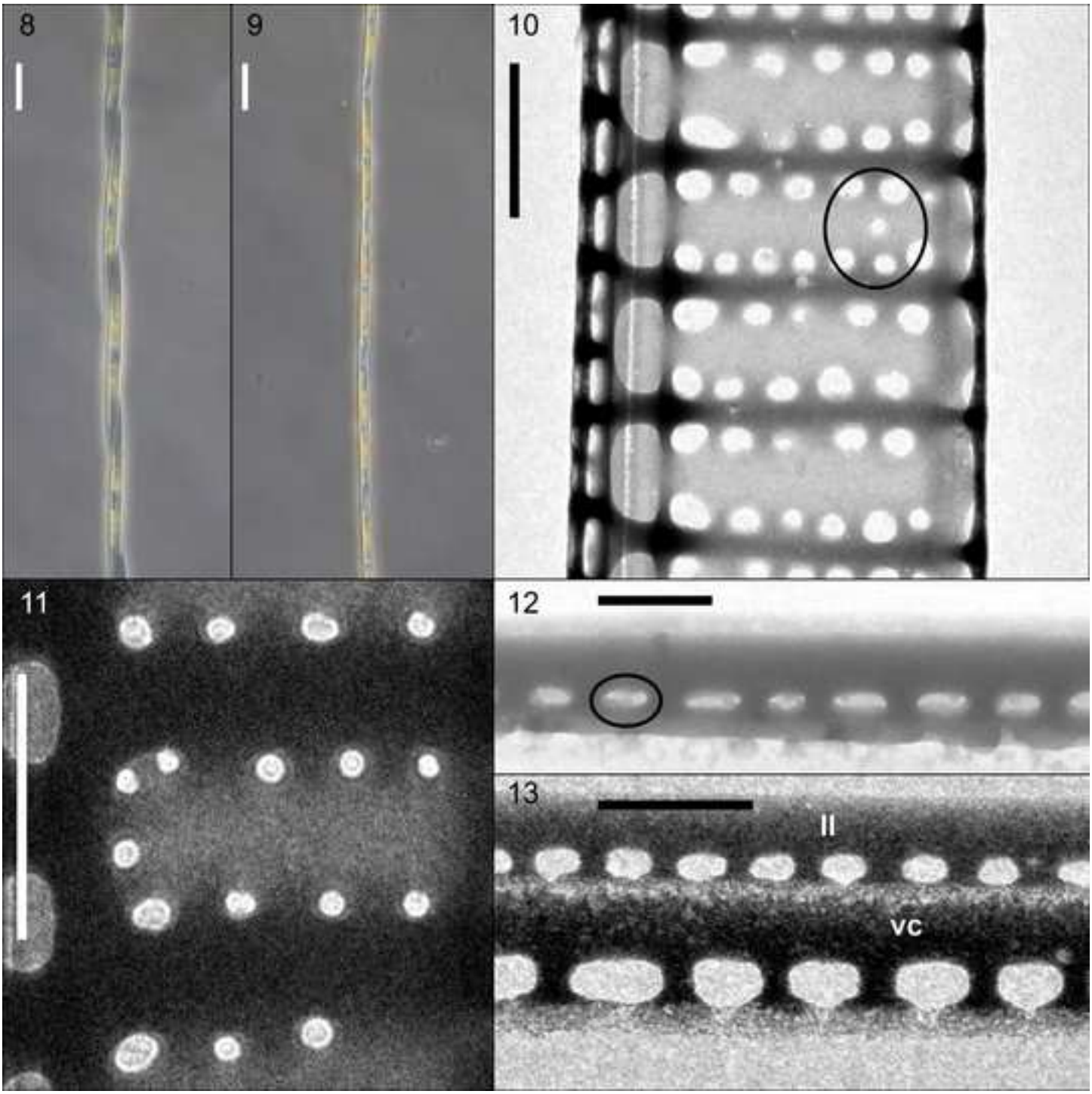

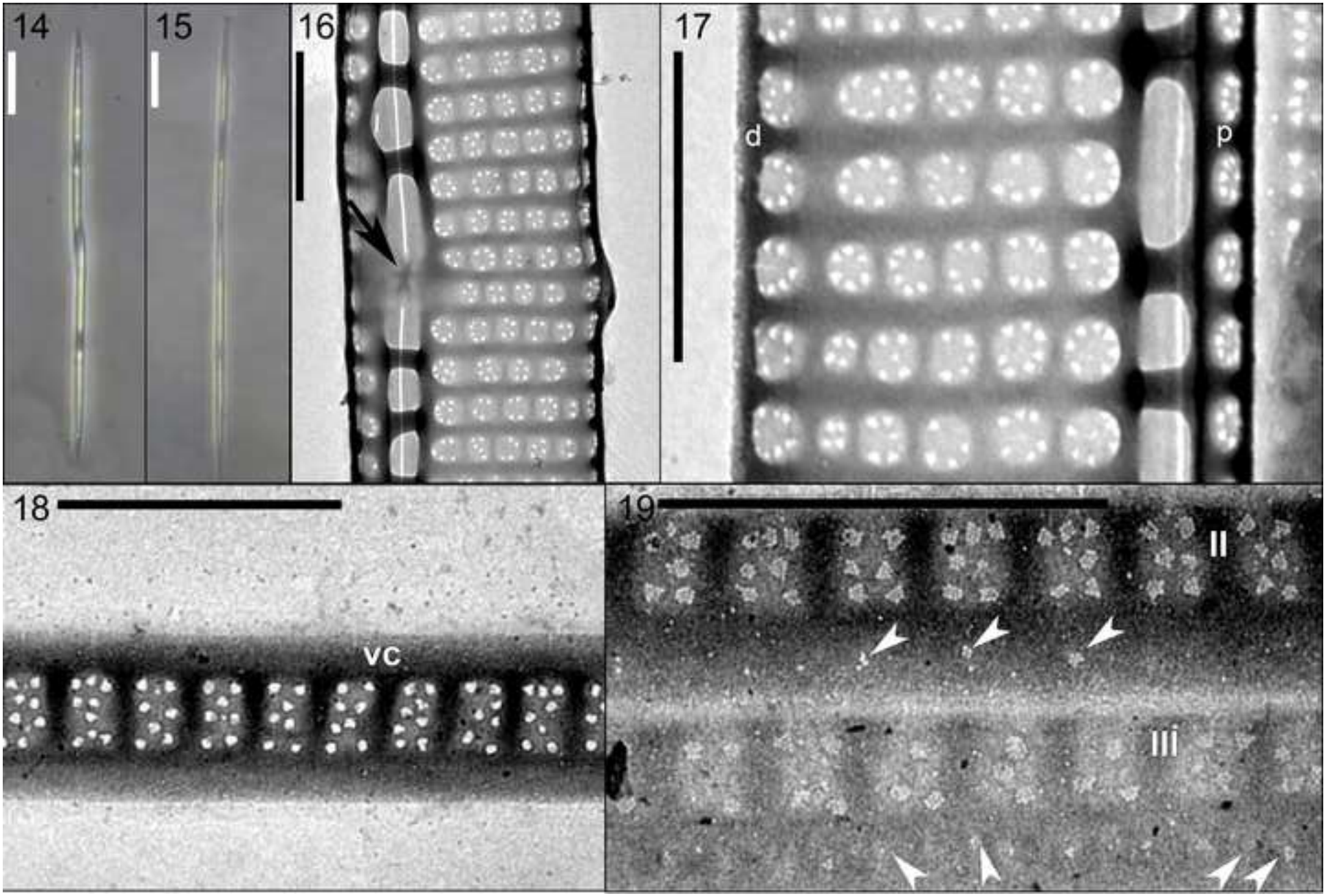

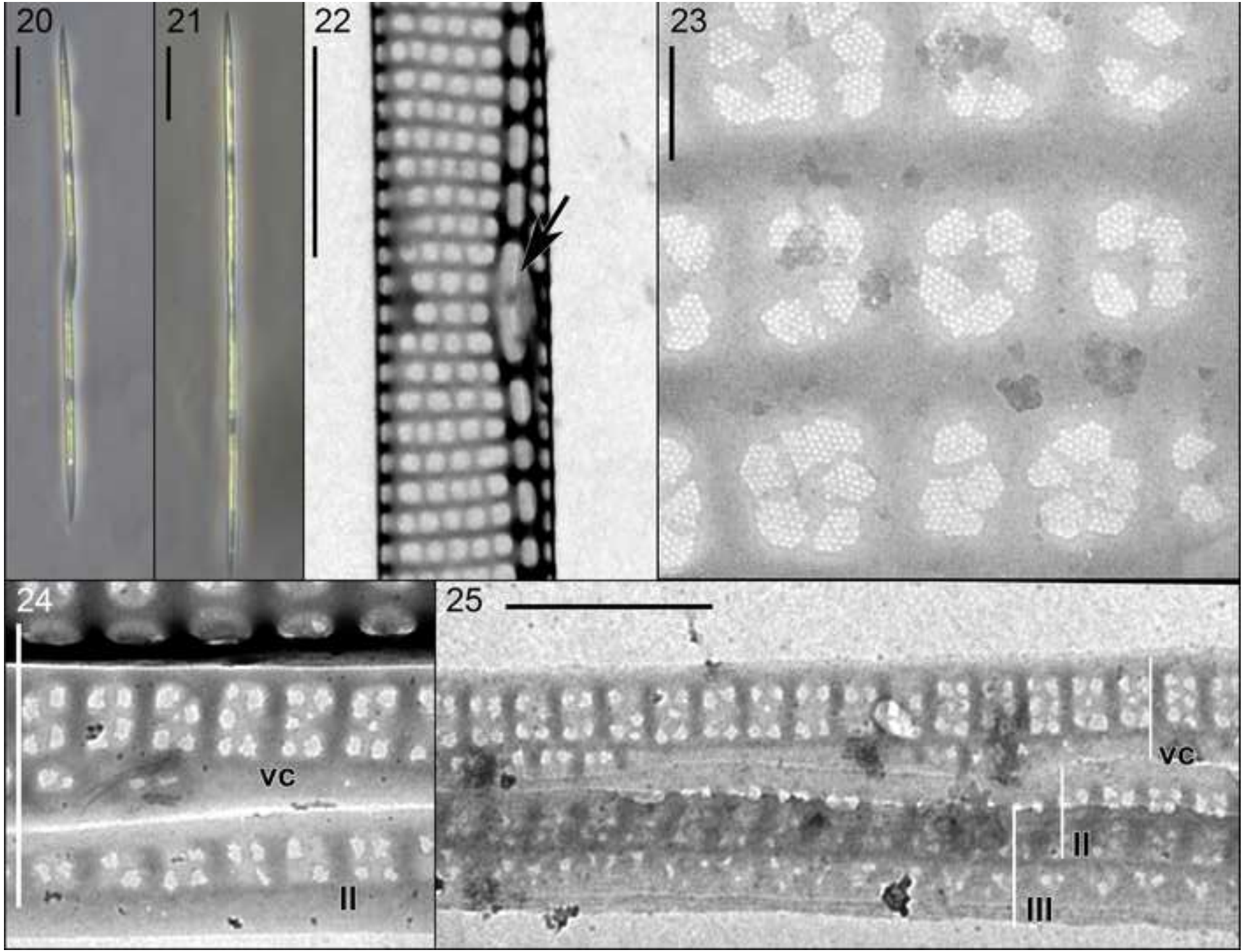

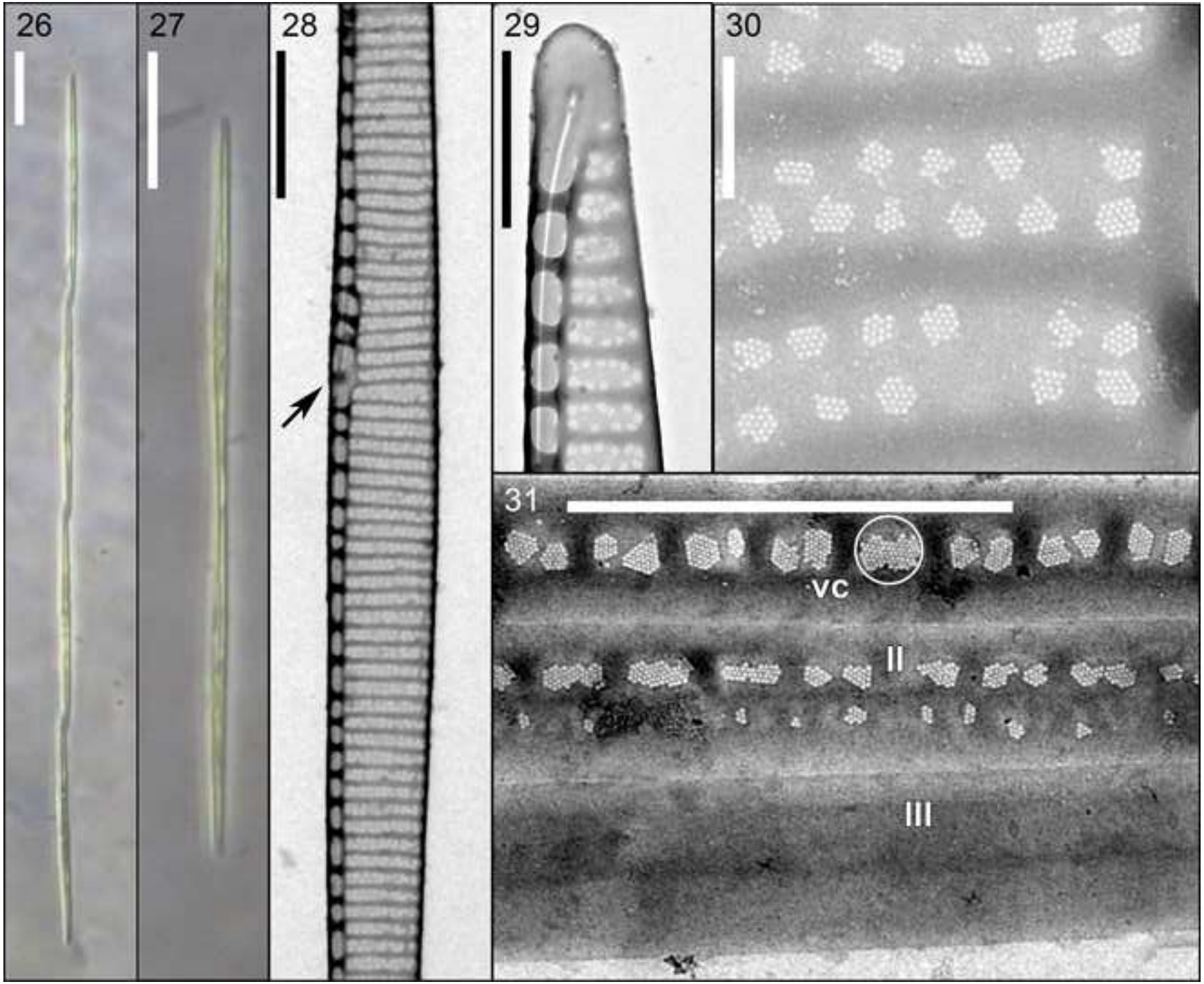

Figs 32-38

Click here to access/download;Figure;Figs 32-38 rev.tif

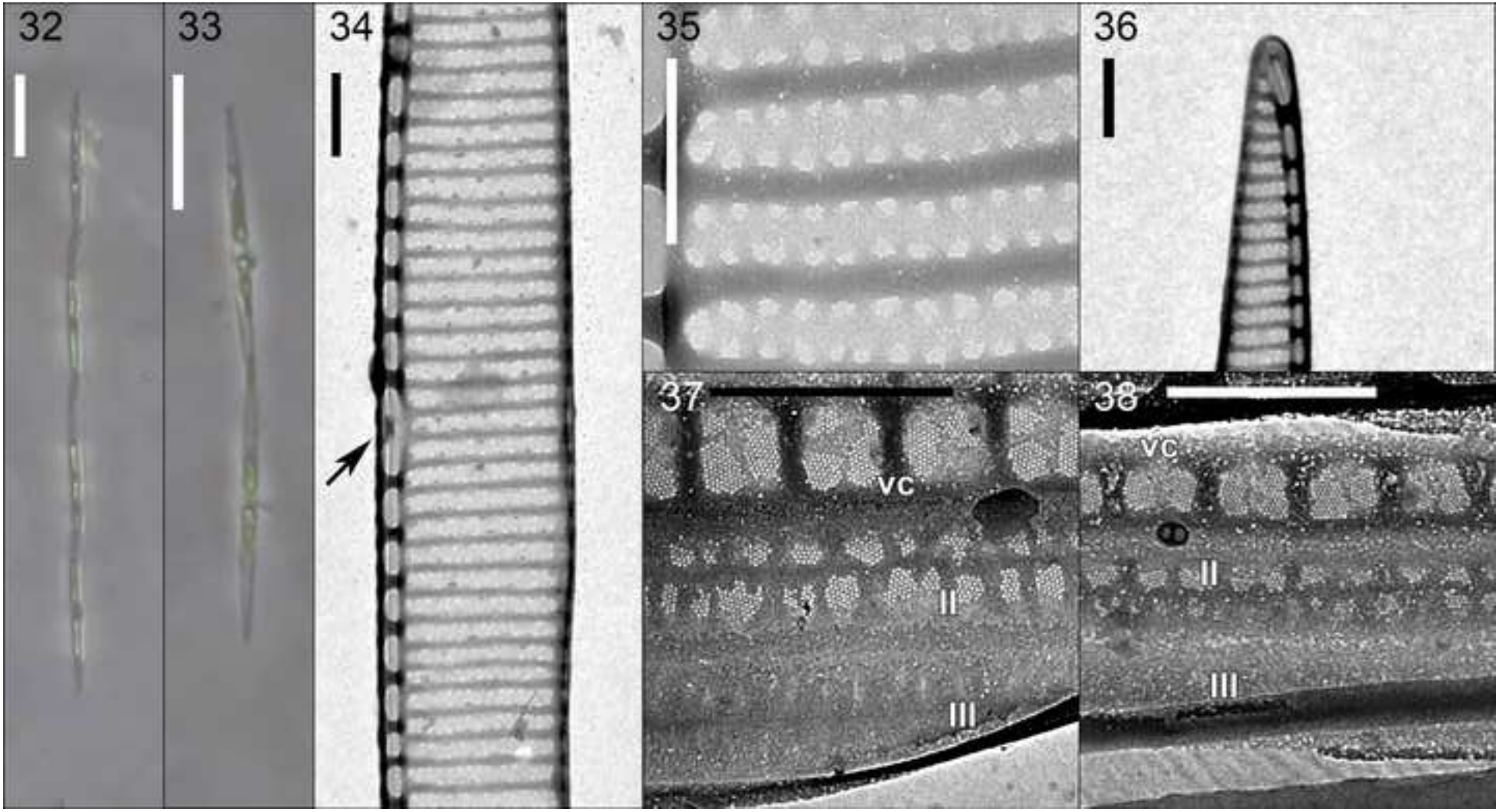

Fig. 39

Click here to access/download;Figure;Fig 39 REV.tiff

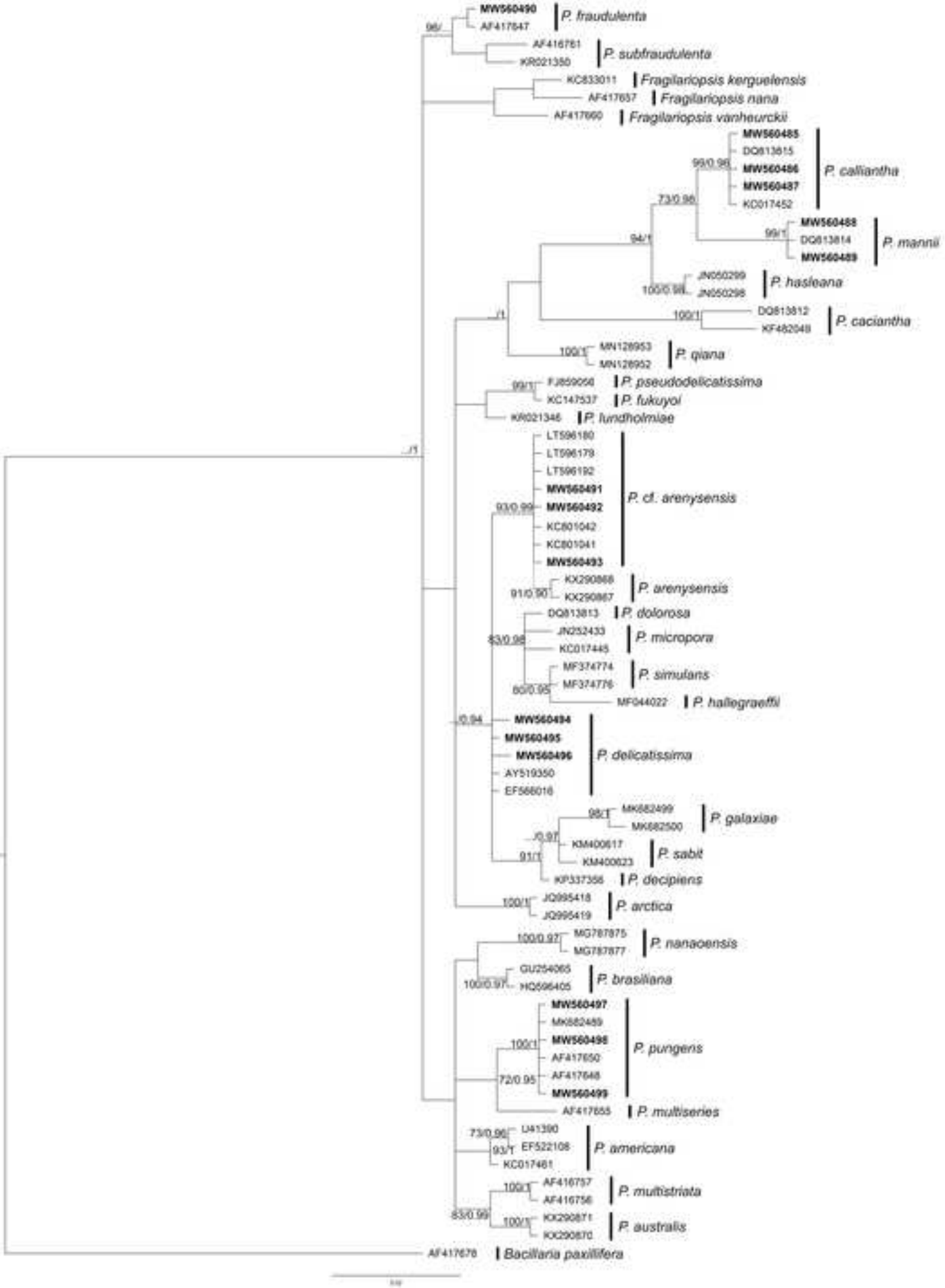

Fig. 40

Click here to access/download;Figure;Fig 40 REV.tiff

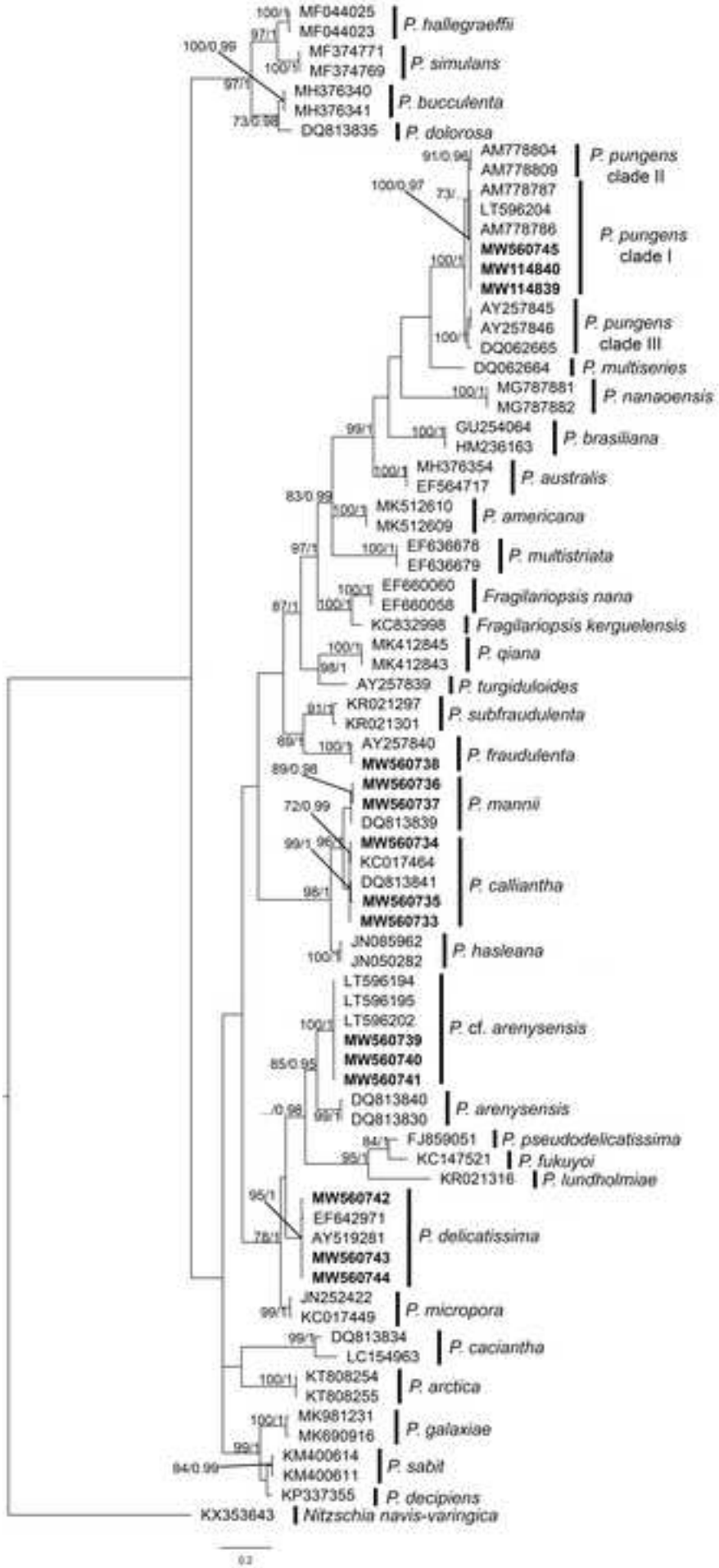

Fig. 41